J. R. Rice[1]

Mechanics of Crack Tip Deformation and Extension by Fatigue

REFERENCE: J. R. Rice, **"Mechanics of Crack Tip Deformation and Extension by Fatigue,"** *Fatigue Crack Propagation, ASTM STP 415,* Am. Soc. Testing Mats., 1967, p. 247.

ABSTRACT: This paper surveys the continuum mechanics of deformation near cracks and its application to propagation by fatigue loadings. Results of various elastic-plastic models are summarized and compared in relation to hardening behavior, size effects, and large scale plastic yielding. The role of the elastic stress intensity factor variations in governing local plastic flow, and thus crack growth rates, is emphasized for the common high-cycle low-stress fatigue situations. General features of crack propagation are discussed, and theories are examined which seek to relate continuum analyses to separation mechanisms.

KEY WORDS: fatigue (materials), crack propagation, fracture mechanics, plasticity, strain concentrations, size effect, hardening

This work views crack propagation as primarily a problem in continuum mechanics. Part I surveys the elastic and elastic-plastic stress analyses of cracked bodies, with emphasis on the plasticity. In addition to well-known results based on models of perfectly plastic anti-plane shearing and discrete surfaces of tensile yielding or slip (equivalently, continuous dislocation arrays), some recently obtained results on work-hardening and anisotropic perfect plasticity are summarized, and methods are presented for the modeling of plane strain yielding. Emphasis is placed on the common result of all plasticity analyses that the coefficient of a characteristic singularity in elastic solutions determines the plastic deformation in situations of small scale yielding. The influences of hardening behavior, finite width effects, and large scale yielding are illustrated and the predictions of various models compared.

Part II considers the mechanics of fatigue crack propagation. Elastic-plastic responses to cyclic loading are determined for perfectly plastic

[1] Assistant professor of engineering, Brown University, Providence, R. I.

and a type of stable hardening behavior. Effectively, the yield stress is doubled so that cyclic flow zones and variations in plastic deformations are smaller than for monotonic loading. Crack tip blunting by large deformations and related effects are treated approximately. General features of fatigue crack growth are surveyed, and the extensive evidence is cited supporting a primary conclusion of continuum analyses: that crack growth rates are determined by elastic stress intensity factor variations for the small scale yielding situation common in low-stress high-cycle fatigue. Results pertaining to mean load, sheet thickness, and mode transition effects, delays in crack extension due to overloads, growth under bending loads, and growth by random applied loads are also noted and interpreted in continuum terms. Theories of crack growth relating continuum considerations to "damage" accumulation and material separation are examined. Further progress requires better continuum analyses, incorporating crack blunting by deformation, and clearer ideas of separation mechanisms.

Part I Continuum Mechanical Description of Deformation Near Cracks

The fundamental importance of the origin, stable growth, and final propagation of cracklike flaws in material failure has stimulated a rapidly increasing amount of research on continuum mechanical descriptions of the stress and deformation fields in cracked bodies. Advances in the elastic and elastic-plastic modelling of crack tip deformations for various geometries and methods of loading are summarized in this part of the paper, and applications of these results in establishing a mechanics of fatigue crack propagation are discussed in Part II. Primary attention is given to elastic-plastic stress analyses, as no survey of the considerable (but as yet far from complete or even reasonably satisfactory) work in this area is currently available and several excellent surveys of the purely elastic treatment of stress concentrations (Neuber [*1*],[2] Savin [*2*]), and cracks in particular (Irwin [*3*], Paris and Sih [*4*]), have appeared.

The objectives of continuum analysis in developing a theoretical framework for crack propagation by fatigue or catastrophic fracture are essentially twofold. First, for various methods and histories of loading structures containing cracks of different sizes and orientations, we seek to determine functions of the applied load and geometry which describe the local deformations suffered by material near the crack tip. Postulating dependence of fracture on this local deformation, parameters of importance in crack propagation and expected characteristics may be identified for the organization and analysis of experimental results, and if

[2] The italic numbers in brackets refer to the list of references appended to this paper.

similarities exist in the local deformation fields for a class of configurations, experimental data on one configuration may then be rationally extended to the prediction of behavior of others. As a second objective, we envision continuum solutions as setting the boundary conditions on microstructural processes submerged in the intense deformation field near the crack tip and resulting in material separation, and seek to predict crack propagation behavior on the basis of models for accumulation of "damage" and final separation. As will be seen, considerable progress has and is being made along the lines of this first objective. Although many theories have been proposed (see Part II), it appears that presently the second objective of relating microstructural models of separation to

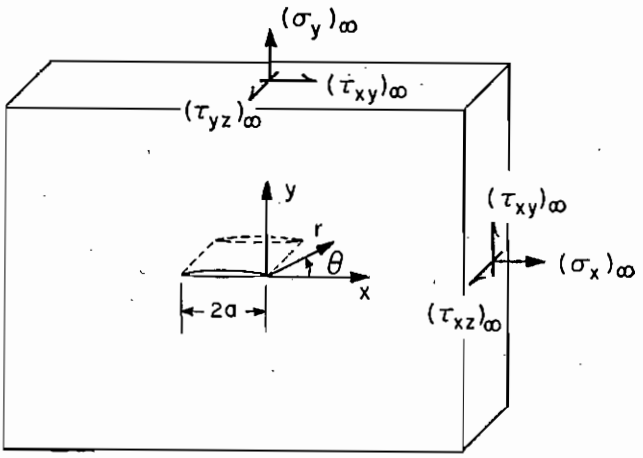

FIG. 1—*Crack of length 2a in infinite plane; uniform stress at infinity.*

continuum deformation analyses, with subsequent predictions of crack growth laws, is inadequately treated.

We begin by considering the elastic analysis of cracks and then take up various plasticity models for crack tip deformation, starting with the case of anti-plane strain, a case of little direct physical interest but one in which the mathematical simplicity allows gaging the effect of various types of plastic behavior. Then models based on discrete surfaces of yielding or slip, which appear most appropriate for plane stress, and a new model based on a slip line field for plane strain are considered. Originally elastic-plastic solutions for monotonically increasing loads are given. Solutions for unloading, cyclic loading, and general load-time histories, as of interest in fatigue crack growth, are then given separately in Part II. Only two-dimensional problems are considered, and primarily the case of a single finite crack of length $2a$ in an infinite plane subject to a uniform stress state at infinity (Fig. 1) is treated in detail, although reference is made to several other configurations.

Linear Elastic Stress Analysis of Cracked Bodies

The characteristic feature emerging from *all* linear elastic solutions to problems of cracks in homogeneous isotropic materials is the inverse square root character of the crack tip stress singularity [*4*]. In particular, components of the stress tensor $\sigma_{ij}(\sigma_{xx} = \sigma_x, \sigma_{xy} = \tau_{xy}, \sigma_{yy} = \sigma_y$, etc.) are representable in the form [*4*]:

$$\sigma_{ij} = r^{-1/2} [K_I f_{ij}^{I}(\theta) + K_{II} f_{ij}^{II}(\theta) + K_{III} f_{ij}^{III}(\theta)] \ldots\ldots\ldots (1)$$

$$+ \text{ other terms nonsingular at the crack tip}$$

where, as for example in Fig. 1, r and θ are polar coordinates introduced at the crack tip. Here the symbols I, II, and III pertain, respectively, to parts of the crack tip region stress field corresponding to displacement discontinuities induced along the crack surface in the tensile, in-plane shear, and anti-plane shear directions respectively, as in Fig. 2. The dimensionless functions f_{ij}^{I}, f_{ij}^{II}, and f_{ij}^{III} depend on the orientation angle

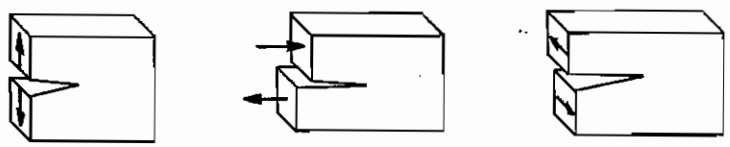

FIG. 2—*Modes of crack tip deformation.*

θ only, and K_I, K_{II}, and K_{III} are the stress intensity factors, introduced into fracture mechanics by Irwin, and again pertaining to the three modes of crack tip deformation. The stress intensity factors may be determined from complete solutions to boundary value problems after an examination of the crack tip stress field and comparison with Eq 1; coming from a linear theory, they must be linear functions of the applied loads. Further, from dimensional considerations the K's have dimensions of $F\,L^{-3/2}$ (F denoting force and L denoting length). Thus if a cracked body is loaded with a remotely applied stress (dimensions of $F\,L^{-2}$) and crack length is the only characteristic length, the K's are proportional to the stress times square root of crack length. If a crack is loaded by a concentrated force per unit thickness (dimensions of $F\,L^{-1}$) applied at the crack center, as for crack branches of equal length emanating from a rivet hole in a sheet, so that crack length remains the only characteristic length, the K's are proportional to the force per unit thickness times the *inverse* square root of crack length. The general conclusion following from Eq 1 is that, to the extent linear elasticity is appropriate, all crack tip stress fields are of identical functional form with the influence of the particular magnitude and method of loading, and geome-

try of the cracked body, sensed in the crack tip region only through the stress intensity factors K_{I}, K_{II}, K_{III}.

For Mode I (tensile) crack tip deformations, the $f_{ij}^{\mathrm{I}}(\theta)$ are readily identified from the equations [4] (with axes as in Fig. 1)

$$\begin{bmatrix} \sigma_y \\ \tau_{xy} \\ \sigma_y \end{bmatrix} = K_{\mathrm{I}}(2\pi r)^{-1/2} \cos(\theta/2) \begin{bmatrix} 1 - \sin(\theta/2)\sin(3\theta/2) \\ \sin(\theta/2)\cos(3\theta/2) \\ 1 + \sin(\theta/2)\sin(3\theta/2) \end{bmatrix} \quad \ldots(2)$$

$$\tau_{xz} = \tau_{yz} = 0,\ \sigma_z = 0 \text{ (generalized plane stress)}$$

$$\sigma_z = \nu(\sigma_x + \sigma_y) \text{ (plane strain, } \nu \text{ is Poisson ratio)}$$

and similar equations may be written for Modes II and III. The stresses $\sigma_y(x, 0)$, $\tau_{xy}(x, 0)$, and $\tau_{zy}(x, 0)$ represent the tractions acting (for $x > 0$) in the y, x, and z directions along the prospective fracture surface. For Mode I

$$\sigma_y(x, 0) = K_{\mathrm{I}}(2\pi x)^{-1/2}, \quad \tau_{xy}(x, 0) = 0,$$

$$\tau_{zy}(x, 0) = 0 \ (\textit{tensile}) \ldots . (3a)$$

for Mode II

$$\sigma_y(x, 0) = 0,\ \tau_{xy}(x, 0) = K_{\mathrm{II}}(2\pi x)^{-1/2},$$

$$\tau_{zy}(x, 0) = 0 \ (\textit{in-plane shear}) \ldots . (3b)$$

and for Mode III

$$\sigma_y(x, 0) = 0, \quad \tau_{xy}(x, 0) = 0,$$

$$\tau_{zy} = K_{\mathrm{III}}(2\pi x)^{-1/2} \ (\textit{anti-plane shear}) \ldots . (3c)$$

For example, with remotely applied stresses and a crack of length $2a$ as in Fig. 1,

$$K_{\mathrm{I}} = (\sigma_y)_\infty(\pi a)^{1/2}, \quad K_{\mathrm{II}} = (\tau_{xy})_\infty(\pi a)^{1/2}, \quad K_{\mathrm{III}} = (\tau_{zy})_\infty(\pi a)^{1/2} \ldots . (4)$$

Other stress intensity factors for a wide variety of crack configurations, including several typical experimental specimens, as well as an exhaustive list of references to workers on elastic crack stress analyses, are cataloged in the paper by Paris and Sih [4].

Limiting attention to two-dimensional problems in homogeneous isotropic materials, Muskhelishvili [5] has shown that for in-plane loadings (Modes I and II) the stresses and displacements are expressible as

$$\left.\begin{aligned}
\sigma_x + \sigma_y &= \sigma_r + \sigma_\theta = 4\,Re\,\{\Phi(\zeta)\} \\
\sigma_y - \sigma_x + 2i\tau_{xy} &= e^{-2i\theta}(\sigma_\theta - \sigma_r + 2i\tau_{r\theta}) = 2\,[\bar{\zeta}\Phi'(\zeta) + \psi(\zeta)] \\
u_x + iu_y &= e^{+i\theta}(u_r + iu_\theta) = \frac{1}{2G}\left\{\kappa\int \Phi(\zeta)\,d\zeta \right. \\
&\qquad \left. - \zeta\overline{\Phi(\zeta)} - \int \overline{\psi(\zeta)\,d\zeta}\right\}
\end{aligned}\right\} \quad \ldots(5)$$

where the equations are given in cartesian and polar form, the u's are displacement components, $\Phi(\zeta)$ and $\psi(\zeta)$ are analytic functions of the complex variable $\zeta = x + iy$, a bar over a quantity denotes its complex conjugate, *Re* means real part, G is the shear modulus, and $\kappa = 3 - 4\nu$ for plane strain and $\kappa = (3 - \nu)/(1 + \nu)$ for generalized plane stress. All other stresses vanish except in the case of plane strain for which $\sigma_z = \nu(\sigma_x + \sigma_y)$. Similarly, for anti-plane loadings (Mode III)

$$\left.\begin{aligned}
\tau_{yz} + i\tau_{xz} &= e^{-i\theta}(\tau_{\theta z} + i\tau_{rz}) = \Omega(\zeta) \\
u_z &= \frac{1}{G}\,Im\left\{\int \Omega(\zeta)\,d\zeta\right\},
\end{aligned}\right\} \quad \ldots\ldots\ldots\ldots(6)$$

with all other stress and displacement components vanishing.

As an example, for the configuration of Fig. 1 with a uniform remote stress state, the complex stress potentials are [5]

$$\left.\begin{aligned}
\Phi(\zeta) &= \tfrac{1}{2}[(\sigma_y)_\infty - i(\tau_{xy})_\infty]\,[\zeta^{-1/2}(\zeta + 2a)^{-1/2}(\zeta + a - 1] \\
&\qquad + \tfrac{1}{2}-[(\sigma_x)_\infty + (\sigma_y)_\infty] \\
\psi(\zeta) &= \bar{\Phi}(\zeta) - \Phi(\zeta) - \zeta\Phi'(\zeta) + \tfrac{1}{2}[(\sigma_y)_\infty - (\sigma_x)_\infty] + i(\tau_{xy_\infty}) \\
\Omega(\zeta) &= (\tau_{yz})_\infty\zeta^{-1/2}(\zeta + 2a)^{-1/2}(\zeta + a) + i(\tau_{xy})_\infty
\end{aligned}\right\} \quad \ldots(7)$$

where $\bar{\Phi}(\zeta) = \overline{\Phi(\bar{\zeta})}$ and the branch cut of $\zeta^{-1/2}(\zeta + 2a)^{-1/2}$ is chosen along the crack line so that the combination behaves as ζ^{-1} for large ζ. That the stress intensity factors for this configuration are correctly given by Eq 4 may be checked by computing the crack tip stresses from Eqs 5 and 6 and comparing with the singular forms of Eqs 3 which serve to define the stress intensity factors. Paris and Erdogan [6] have pointed out the relation between the stress concentration factors popularized by Neuber [1] and Irwin's stress intensity factors. For an ellipse of length $2a$ and end radius of curvature ρ subjected to an in-plane tension $(\sigma_y)_\infty$, the maximum concentrated tensile stress is

$$\sigma_{\max} = (\sigma_y)_\infty[1 + 2(a/\rho)^{1/2}] \ldots\ldots\ldots\ldots\ldots(8a)$$

Similarly, the maximum concentrated shear stress due to an anti-plane shear $(\tau_{yz})_\infty$ is

$$\tau_{max} = (\tau_{yz})_\infty [1 + (a/\rho)^{1/2}] \quad (8b)$$

Comparing these with Eqs 4, for $\rho \ll a$ (narrow ellipse) the maximum concentrated stresses and stress intensity factors are related by

$$K_I = \tfrac{1}{2}(\pi\rho)^{1/2}\sigma_{max} \quad (8c)$$

in the tensile mode, and by

$$K_{III} = (\pi\rho)^{1/2}\tau_{max} \quad (8d)$$

in the anti-plane shear mode.

To the extent that inelastic behavior is of no major influence, the surrounding elastic crack tip stress fields are identical for two configurations if their stress intensity factors are equal, and thus if material properties are identical, the stress and deformation distributions in the inelastic regions are presumably identical. This conclusion of elastic stress analysis is of obvious importance; it embodies a large part of the progress

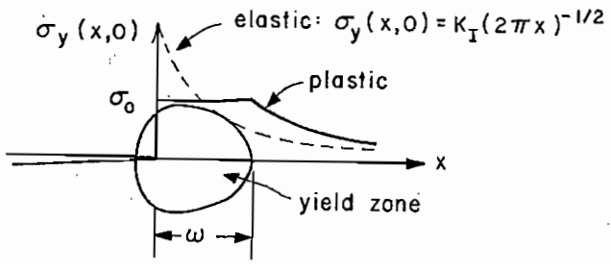

FIG. 3—*Approximate calculation of plastic zone size.*

of modern fracture mechanics. The deficiencies of purely elastic analysis are equally clear, necessitating analyses based on more realistic material models allowing for plastic flow. Quantitative estimates of when the elastic singularity controls local deformations are needed and new parameters must be established as controlling these deformations when plasticity is on a large enough scale to wipe out the characteristic surrounding elastic field. The physical differences between plane strain and plane stress states, very significant in the presence of plastic yielding, are inadequately reflected in purely elastic treatments. Details of stress and strain distributions in separation prone material at the crack tip obviously require a plasticity treatment for reasonable descriptive accuracy. Serious crack blunting can only result from large strains of plastic, not elastic, magnitude. Finally, plastic deformations are history dependent and elastic deformations are not of particular significance in fatigue where separations result from nonmonotonic deformation histories.

Rough estimates of the scale of plasticity are obtainable from simple manipulations based on the elastic stress field. Consider the tensile mode as depicted in Fig. 3 and suppose that the plastic region, of linear di-

mension ω, is imbedded in the field of the elastic singularity. Let σ_o be an effective yield stress, as modified by a degree of hardening or by hydrostatic stresses. As in Fig. 3, the yielded region should extend over roughly twice (due to stress redistribution) the distance from the crack tip at which the dashed line singular elastic stress field equals the yield stress. Then from Eq 3*a*,

$$\sigma_o = \sigma_y(\omega/2, 0) = K_I(2\pi\omega/2)^{-1/2}; \qquad \omega = \frac{1}{\pi}\frac{K_I^2}{\sigma_o^2} \ldots\ldots\ldots (9)$$

This estimate of plastic zone size is surprisingly accurate for well contained plasticity. Similar formulas follow for the shear modes with σ_o replaced by τ_o, a yield stress in shear.

The plastic zone size (Eq 9) establishes a geometric dimension indi-

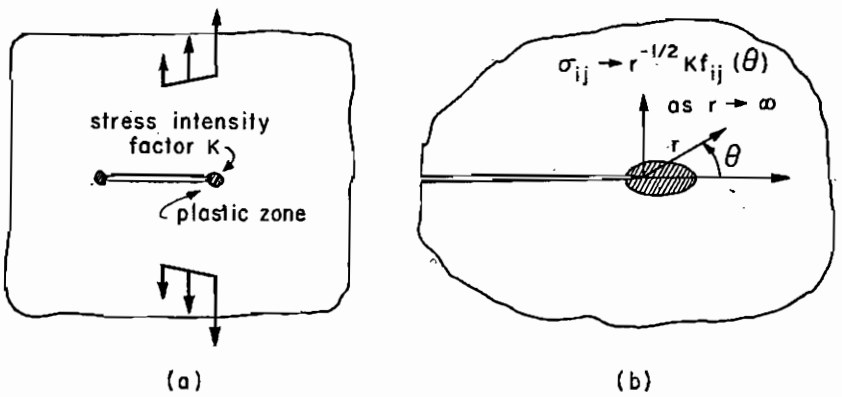

FIG. 4—*Small scale yielding near crack; crack may be viewed as semiinfinite with inverse square root stresses approaches at large distances.*

cating the region over which deviations from elastic behavior occur. Now the characteristic length associated with the elastic stress field is a dimension such as crack length, uncracked width of a finite specimen, distance from crack tip to points of load application, and so forth. Thus at load levels sufficiently low so that the plastic zone size computation of Eq 9 gives a length small compared to all such dimensions, the plasticity may be expected controlled by the elastic stress intensity factor. We call this situation "small scale yielding." Conversely, when the length predicted by Eq 9 is comparable to or greater than such geometric dimensions, a correction to Eq 9 is required as the stress intensity factor may no longer be expected to control the plasticity. These conclusions are borne out in all the plasticity models examined subsequently. As might be expected, the nonlinearity inherent in elastic-plastic analysis causes considerable complexity in the determination of deformation distributions even for the simplest of models. Since our interest is frequently in situations of small scale yielding where the stress intensity factor dominates, it is of interest to inquire as to whether simpler analyti-

cal methods may be established valid only for this case and not for the entire range of large scale yielding. A concept of a boundary layer approach has emerged in this connection in some recent work by the author [*7–10*]. In the limit when plastic region dimensions are negligible compared to geometric dimensions, the surrounding elastic singularity sets the boundary conditions on the elastic-plastic boundary value problem, in the sense that the plastically yielding material only "sees" the surrounding stress field through the inverse square root term in the elastic solution, this stress field being approached by the elastic-plastic solution at distances large compared to the plastic zone size but still small compared to other geometric dimensions. Thus the small scale yielding solution for any loading (Fig. 4*a*) may be obtained by considering a semi-infinite crack (Fig. 4*b*) with the asymptotic boundary conditions that the inverse square root elastic stress field is approached at large distances:

$$\sigma_{ij} \to r^{-1/2} K f_{ij}(\theta) \quad \text{as} \quad r \to \infty \ldots\ldots\ldots\ldots \quad (10)$$

Here K is the stress intensity factor pertaining to the particular manner of loading and deformation mode.

Letting $\Phi_s(\zeta)$, $\psi_s(\zeta)$, and $\Omega_s(\zeta)$ denote the form of the complex stress potentials when only the singular term is included,

$$\Phi_s(\zeta) = 2\psi_s(\zeta) = \frac{K_{\mathrm{I}}}{2(2\pi\zeta)^{1/2}}, \Omega_s(\zeta) = 0, \text{(tensile)} \ldots\ldots\ldots\ldots\ldots \text{(11a)}$$

$$\Phi_s(\zeta) = -\frac{2}{3}\psi_s(\zeta) = -\frac{iK_{\mathrm{II}}}{2(2\pi\zeta)^{1/2}}, \Omega_s(\zeta) = 0, \text{(in-plane shear)} \ldots \text{(11b)}$$

$$\Phi_s(\zeta) = \psi_s(\zeta) = 0, \Omega_s(\zeta) = \frac{K_{\mathrm{III}}}{(2\pi\zeta)^{1/2}}, \text{(anti-plane shear)} \ldots\ldots\ldots \text{(11c)}$$

where the crack tip is at $\zeta = 0$ and the crack surface extends along the negative real ζ axis. The asymptotic boundary condition for small scale yielding is equivalent to requiring that the complex potentials approach the appropriate above form as $|\zeta| \to \infty$.

Anti-Plane Shearing

The third mode of crack tip deformation, anti-plane shearing, is of little practical importance as fatigue cracks generally tend to initiate (if not already present) through an in-plane shearing mode involving repeated deformation in slip bands [*11,12*], and to propagate in a tensile mode. The motivation for dealing with this case is primarily the lack of comparable progress in the analysis of the tensile mode. Exact mathematical solutions are now available for the anti-plane shearing of cracks in perfectly plastic materials, including both plastically isotropic (Tresca or Mises yield condition [*13*] governing) and anisotropic (including the

special case of single crystals with discrete slip directions) materials, and for work hardening materials with arbitrary relations between principal shear stress and shear strain in the work hardening range. Attempts at drawing direct analogies between *detailed* features of anti-plane shearing and tensile crack tip deformation fields appear largely unjustified. However, the two cases share commonly the principal features of load transmission around a traction free surface in materials which will support limited stresses, and since Eqs 3, 4, and 8 predict notable similarities in purely elastic response, one confidently expects analogies between *gross* features of plasticity effects in the anti-plane and tensile modes. Thus, for example, anti-plane predictions of the dependence of plastic zone sizes and crack opening displacements on applied loads and geometrical dimensions, as well as general conclusions drawn from variations of the yield surface and introduction of hardening

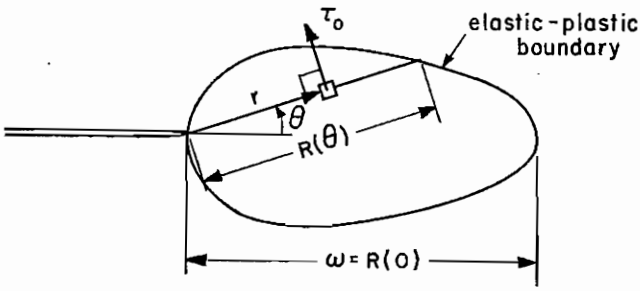

FIG. 5—*Yielded region near crack in perfectly plastic Tresca or Mises material subjected to anti-plane shearing.*

behavior, are likely good approximations for the tensile case. McClintock and Irwin [*14*] have recently discussed this point.

Hult and McClintock [*15*] gave the form of the stress and strain distribution in the plastic region adjoining the crack tip for a perfectly plastic material satisfying the Tresca or Mises yield condition (coincident in this case),

$$\tau_{xz}^2 + \tau_{yz}^2 \leqslant \tau_o^2 \quad \ldots\ldots\ldots\ldots\ldots\ldots\ldots\ldots (12a)$$

that the principal shear stress not exceed the yield stress τ_o. Referring to Fig. 5, in the plastic zone

$$\left.\begin{aligned} &\tau_{\theta z} = \tau_o \,,\ \tau_{rz} = 0 \\ &\gamma_{\theta z} = \frac{1}{r}\frac{\partial u_z}{\partial \theta} = \gamma_o \frac{R(\theta)}{r} \,,\ \gamma_{rz} = \frac{\partial u_z}{\partial r} = 0 \\ &u_z = \gamma_o \int_0^\theta R(\psi)\, d\psi \end{aligned}\right\} \quad \ldots\ldots\ldots (12b)$$

where $\gamma_o = \tau_o/G$ is the yield strain and $R(\theta)$ is the radial distance to the elastic-plastic boundary. The plastic zone size, ω, and crack opening displacement, u_o, are

$$\omega = R(0), u_o = u_z|_{\theta=\pi 2, r=0} = \gamma_o \int_0^{\pi/2} R(\theta)d\theta \ldots\ldots (12c)$$

The small scale yielding solution for this case was first found by Hult and

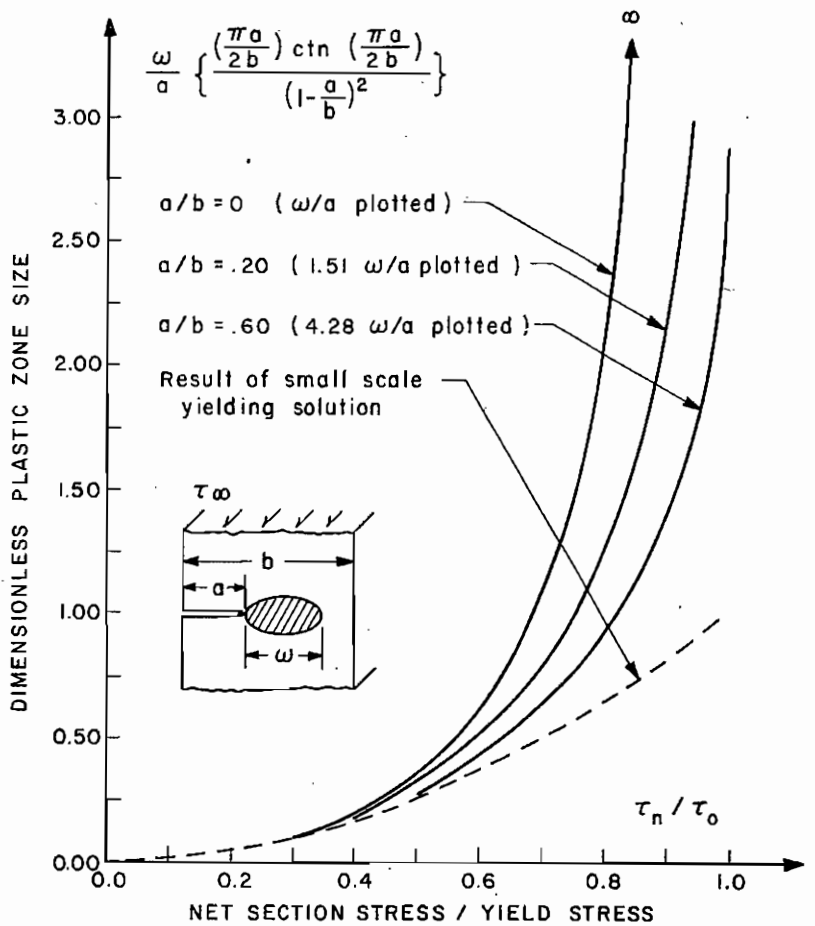

FIG. 6—*Plastic zone size as a function of net section stress for various crack length to width ratios; anti-plane shearing of perfectly plastic Tresca or Mises material.*

McClintock [*15*] and further elaborated by Irwin and Koskinen [*16*] and Rice [*8*]. The plastic zone is circular in shape with

$$R(\theta) = \omega \cos\theta;\ \omega = \frac{K_{III}^2}{\pi\tau_o^2} \approx 0.318\,\frac{K_{III}^2}{\tau_o^2} \ldots\ldots (13a)$$

$$u_o = \frac{\gamma_o K_{III}^2}{\pi\tau_o^2} = \gamma_o\omega \ldots\ldots (13b)$$

Shear stresses in the elastic region outside the circular plastic zone are given by [*8,16*]

$$\tau_{yz} + i\tau_{xz} = \Omega(\zeta) = \frac{K_{III}}{[2\pi(\zeta - \omega/2)]^{1/2}} \quad \ldots\ldots\ldots (13c)$$

Comparing with Eq 11*c*, the effect of plasticity is to shift the purely elastic stress distribution ahead by half the plastic zone size.

For the crack of length $2a$ in an infinite body configuration of Fig. 1,

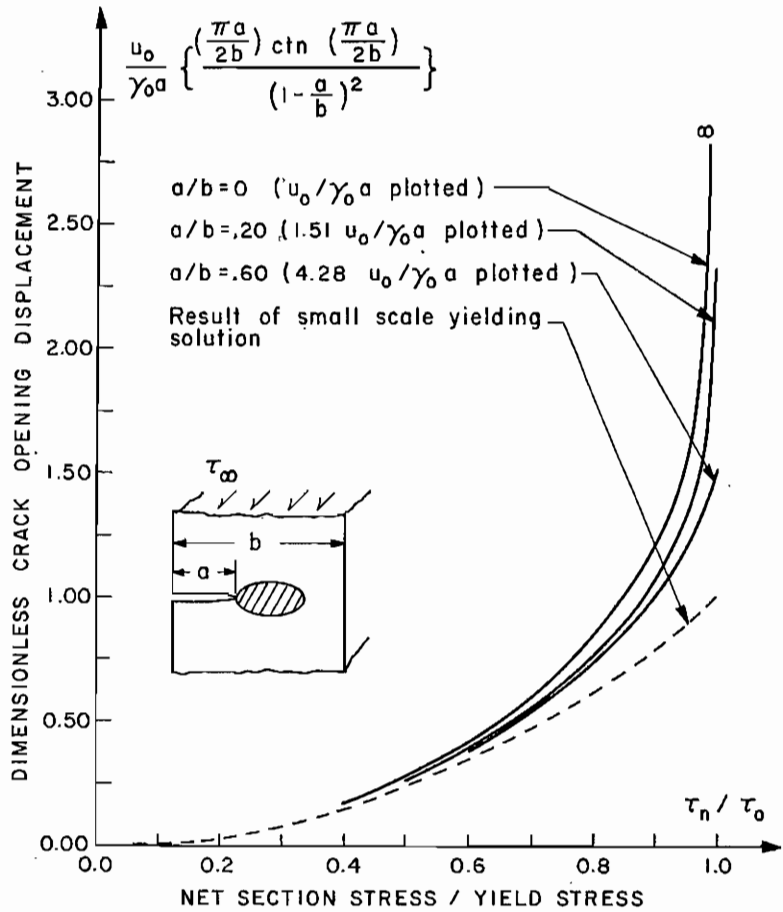

FIG. 7—*Crack opening displacement as a function of net section stress for various crack length to width ratios; anti-plane shearing of perfectly plastic Tresca or Mises material.*

loaded with a single remotely applied anti-plane shear stress $(\tau_{yz})_\infty = \tau_\infty$, the plastic zone size and crack opening displacement are [*8,15*]

$$\omega = a\left[\frac{2}{\pi}\frac{1+s^2}{1-s^2}E_2\left(\frac{2s}{1+s^2}\right) - 1\right] \quad \ldots\ldots\ldots (14a)$$

$$u_o = \gamma_o a\left[\frac{2}{\pi}(1+s^2)E_1(s^2) - 1\right] \quad \ldots\ldots\ldots (14b)$$

where $s = \tau_\infty/\tau_o$ and E_1, E_2 are complete elliptic integrals of the first and second kind. Noting that $K_{III} = \tau_\infty(\pi a)^{1/2}$, these may readily be shown to reduce to the small scale yielding results of Eq 13*a* at low stress levels. The shape of the plastic zone is initially circular and it elongates much as in Fig. 5 at higher stress levels until at the limit load $\tau_\infty = \tau_o$ the zone extends to infinity in the x direction with a height in the y direction approaching [*8*] asymptotically to $4a/\pi$. Koskinen [*17*] first treated the configuration of Fig. 1 for the case of a finite, rather than infinite, width in the x direction. While his solution was based on a numerical finite-difference scheme, Rice [*8*] later provided an analytic solution. When the width is $2b$ and the crack is centrally located the stress intensity factor is [*4*]

$$K_{III} = \tau_\infty(\pi a)^{1/2}\left[\frac{2b}{\pi a}\tan\left(\frac{\pi a}{2b}\right)\right]^{1/2} \quad \ldots\ldots\ldots\ldots (15a)$$

The same solution applies for an edge crack of length a in a plane of width b, or for double edge notches of depth a in a plane of width $2b$. These configurations are only approximately equivalent in the tensile case (for example, $K_I \approx 1.1\ \sigma_\infty(\pi a)^{1/2}$ for an edge crack in an infinite plane). The bracketed term of Eq 15*a* provides a good approximation, which can be improved upon [*4*], to the finite width correction in the tensile case. The graphs of Figs. 6 and 7 give dimensionless plots of the plastic zone size and crack opening displacement for several crack length to thickness ratios, a/b, in terms of the ratio of the *net* section stress, $\tau_n = \tau_\infty(1 - a/b)^{-1}$, to the yield stress. Using Eqs 13*a*, 13*b*, and 15*a*, the small scale yielding solution for which the stress intensity factor dominates leads to

$$\omega = \frac{u_o}{\gamma_o} = a\left(1 - \frac{a}{b}\right)^2\left[\frac{2b}{\pi a}\tan\left(\frac{\pi a}{2b}\right)\right]\left(\frac{\tau_n}{\tau_o}\right)^2 \quad \ldots\ldots\ldots (15b)$$

The dimensionless plastic zone size

$$\frac{\omega}{a}\frac{\left(\frac{\pi a}{2b}\right)\mathrm{ctn}\left(\frac{\pi a}{2b}\right)}{\left(1 - \frac{a}{b}\right)^2}$$

appears as a function of dimensionless net section stress, τ_n/τ_o, in Fig. 6 for crack length to plane thickness ratios, a/b, of 0, 1/5, and 3/5. The dimensionless crack opening displacement

$$\frac{u_o}{\gamma_o a} \frac{\left(\frac{\pi a}{2b}\right) \operatorname{ctn}\left(\frac{\pi a}{2b}\right)}{\left(1 - \frac{a}{b}\right)^2}$$

appears as a function of the same parameters in Fig. 7. From Eq 15*b*, both of these dimensionless parameters equal the square of the net

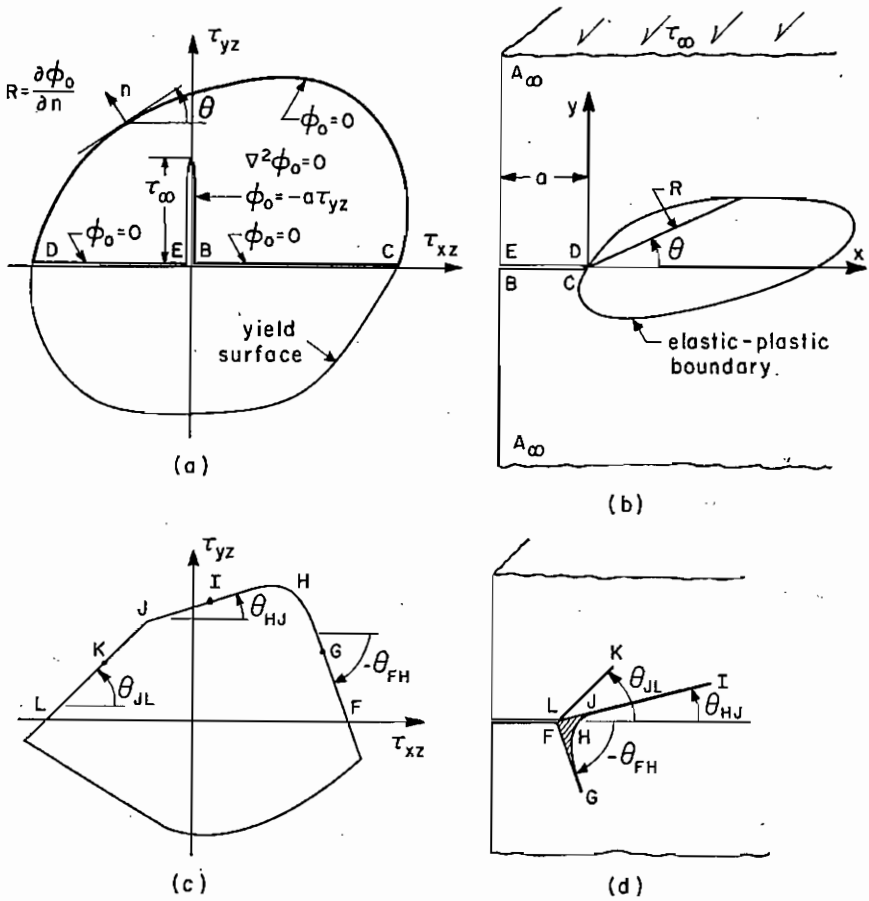

FIG. 8—(a *and* b) *General formulation for anti-plane shearing of elastic perfectly plastic material with crack;* (c *and* d) *special features of solution when yield surface contains straight line segments corresponding to restricted slip directions (discrete slip lines) formed at crack tip).*

section stress to yield stress ratio according to the small scale yielding solution, and this is shown by the dashed lines. The heavy lines are the results of exact computations [*8*] which do not make the small scale yielding approximation. The bracketed factor in the above two-dimensionless expressions equals 1.00 for $a/b = 0$, 1.51 for $a/b = 0.20$, and 4.28 for $a/b = 0.60$, as indicated on the graphs.

Considering Fig. 6 first, prediction of the plastic zone size by the small scale yielding solution (Eq 15*b*) is seen to be accurate up to 30 per cent of the limit load ($\tau_n/\tau_o = 1$) for $a/b = 0$, up to 40 per cent for $a/b =$

0.20, and up to 50 per cent for $a/b = 0.60$. At higher stress levels the stress intensity factor is not even approximately descriptive of local conditions at the crack tip. It should be cautioned that these results are for monotonic loading only. As will be seen later, cyclic loadings as for fatigue produce a smaller zone of cyclic plastic deformation for which the same curves are valid but with τ_n/τ_o replaced by the cyclic variation in net section stress divided by *twice* the yield stress, so that the stress intensity factor is descriptive of local *cyclic* conditions up to much higher stress levels. The crack opening displacement (Fig. 7) is seen to be accurately predicted by the small scale yielding formula (Eq 15*b*) up to much higher stress levels, with the stress intensity factor failing to be descriptive of local conditions above about 60 to 70 per cent of the limit load.

Rice [*10*] has recently generalized the procedures employed [*8*,*15*,*17*] for obtaining the solutions discussed above, by formulating the anti-plane shearing problem for perfectly plastic materials with yield surfaces of *arbitrary* convex shape in the two-dimensional τ_{xz}, τ_{yz} shear stress space (the Tresca or Mises yield condition (Eq 12*a*) then being the special case of a circle of radius τ_o in this space). The principal features of the solution for an edge crack of depth a in an infinite body (or equivalently the crack of length $2a$ in an infinite body configuration of Fig. 1), subjected to a remotely applied anti-plane shear stress τ_∞, are summarized in Fig. 8. A yield surface appears in Fig. 8*a*, the cracked body in Fig. 8*b*. For the remotely applied stress in the direction shown, stresses in the plastic zone correspond to points on the upper part ($\tau_{yz} > 0$) of the yield surface. When the yield surface contains no straight line segments the stress components are constant along radial lines in the plastic zone, so that along a line from the crack tip making an angle θ with the x axis the stresses have those values corresponding to the point on the yield surface for which the tangent line makes the same angle θ with the τ_{xz} axis. Strains exhibit a $1/r$ singularity at the crack tip, and the plastic part of the strain has a direction perpendicular to the radial lines. The elastic portion of the physical x, y plane may be shown [*10*] to map into the region of the stress plane between the τ_{xz} axis and the upper part of the yield surface, with corresponding points as labeled by the capital letters in Figs. 8*a* and *b*. An inverse solution for physical coordinates in the elastic region as a function of stress follows by introducing a potential function $\phi_o = \phi_o(\tau_{xz}, \tau_{yz})$. Then

$$x = -\frac{\partial \phi_o}{\partial \tau_{yz}}, y = +\frac{\partial \phi_o}{\partial \tau_{xz}}, \text{ and } \nabla^2 \phi_o = \frac{\partial^2 \phi_o}{\partial \tau_{xz}^2} + \frac{\partial^2 \phi_o}{\partial \tau_{yz}^2} = 0 \ldots (16a)$$

and the harmonic function ϕ_o vanishes on the τ_{xz} axis and the upper part of the yield surface, as in Fig. 8*a*. Along the τ_{yz} axis from the origin out to a stress distance equal to the remotely applied stress,

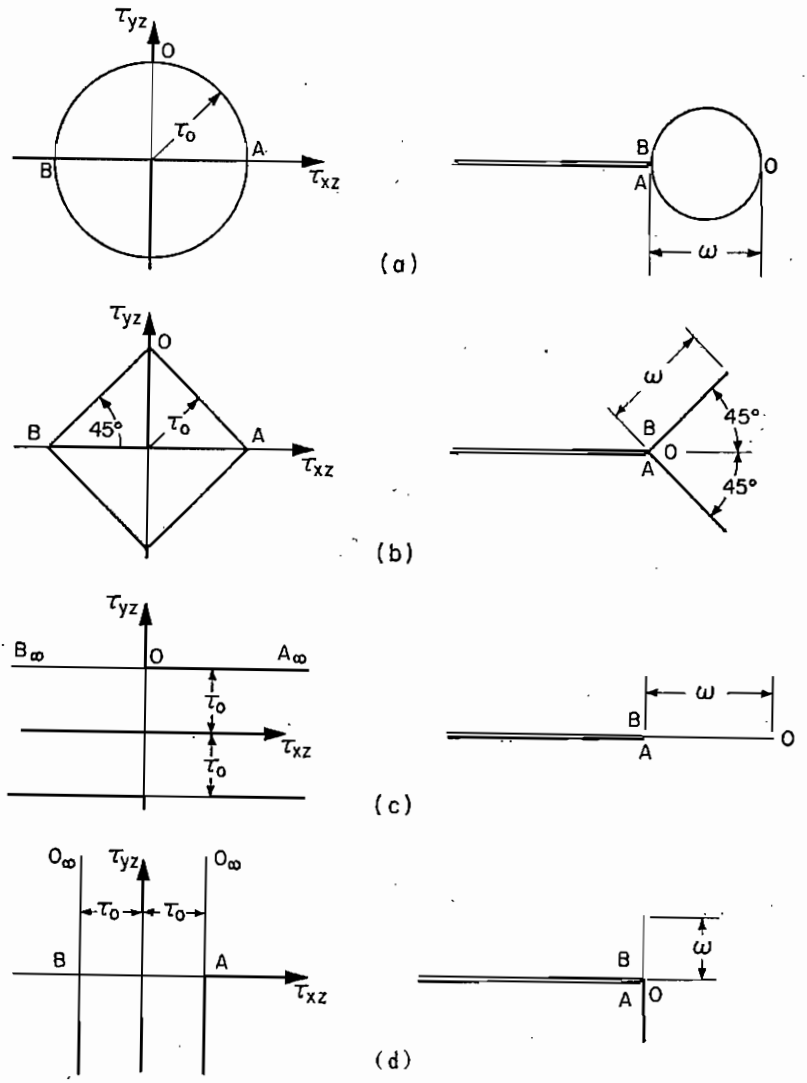

FIG. 9—*Small scale yielding solutions for anti-plane shearing of perfectly plastic materials:* (a) *Tresca-Mises material,* (b) *orthogonal allowed slip directions at 45 deg with crack line, and* (c *and* d) *single allowed slip directions.*

$$\phi_o = -a\,\tau_{yz}\,, \qquad 0 < \tau_{yz} < \tau_\infty \quad \ldots\ldots\ldots\ldots (16b)$$

The distance R from the crack tip to a point on the elastic plastic boundary, corresponding to a given point on the yield surface, is found from [*10*]

$$R = \frac{\partial \phi_o}{\partial n}$$

where $\partial\phi_o/(\partial n)$ is the derivative of ϕ_o in the direction normal to the yield surface. A membrane analogy is readily established allowing effective visualization of the solution; ϕ_o may be viewed as the deflection of a membrane subjected to zero transverse pressure and stretched out over an opening in a sheet corresponding to the region between the upper

part of the yield surface and the τ_{xz} axis of Fig. 8*a*. According to Eq 16*b*, the membrane is loaded by bringing a thin wire of length corresponding to τ_∞ into contact with the membrane along the τ_{yz} axis, such that the wire has a downward slope corresponding to crack length a. Equation 16*c* then indicates that the distance R to a point on the elastic plastic boundary corresponds to the slope of the membrane in the direction normal to its fixed boundary. Thus, for example, it is readily understood that as the remotely applied stress is increased toward the limit load, the plastic zone tends to elongate in a direction corresponding to the yield surface tangent at the point where the yield surface intersects the τ_{yz} axis.

When the yield surface contains straight line segments, as in Fig. 8*c*, the above formulation of Eqs 16 remains valid, but it is now meaningless to speak of plastic strains as the plastic zone coalesces into discrete slip lines across which the anti-plane displacement u_z has a discontinuous jump. As in Figs. 8*c* and *d*, a discrete slip line emanating from the crack tip corresponds to each straight line segment of the yield surface; a continuous field of plastic strain joins separate discrete slip lines when a corner of the yield surface is rounded as at point H of Fig. 8*c*. Straight line segments on the yield surface result when only certain directions of plastic shearing are allowable, as in a single crystal or for events on the scale of a single grain rather than a polycrystalline aggregate. The allowed slip surfaces have the direction of the straight line segment, and the perpendicular stress distance from the origin of the stress plane to the straight line segment is the resolved shear stress required for slip. Studies are currently underway on the relevance of similar conclusions for the tensile deformation of materials with restricted slip directions.

Figure 9 pictures four yield surfaces and the corresponding plastic zones obtained by Rice [*10*] in a solution method developed for small scale yielding. The plastic zone dimension, ω, and crack opening displacement, u_o, have already been given in Eqs 13 for the circular Tresca-Mises criterion of Fig. 9*a*. For the diamond-shaped yield surface of Fig. 9*b*, corresponding to slip under a resolved shear stress τ_o on planes inclined at 45 deg with the crack line, plastic zone size (slip line length) and crack opening displacement are [*10*]

$$\left.\begin{aligned} \omega &= \frac{\lambda^2}{8\pi}(\sqrt{3}-1)\left[\frac{3\sqrt{3}}{2(2-\sqrt{3})}\right]^{1/2}\frac{K_{III}^2}{\tau_o^2} \approx 0.322\,\frac{K_{III}^2}{\tau_o^2} \\ u_o &= \frac{\lambda\gamma_o K_{III}^2}{2\pi\tau_o^2} \approx 0.916\,\gamma_o\omega \end{aligned}\right\} \quad \ldots(17a)$$

where $\lambda \approx 1.8541$ is the complete elliptic integral of the first kind with modulus $\frac{1}{2}$. Allowable slip surfaces are parallel to the crack surface in Fig. 9*c*; in this case

$$\left.\begin{aligned} \omega &= \frac{\pi K_{III}^2}{8\tau_o^2} \approx 0.392 \frac{K_{III}^2}{\tau_o^2} \\ u_o &= \frac{\gamma_o K_{III}^2}{4\tau_o^2} = \frac{2}{\pi} \gamma_o \omega \approx 0.636\, \gamma_o \omega \end{aligned}\right\} \quad \ldots\ldots\ldots\ldots (17b)$$

Similarly, for allowable slip surfaces perpendicular to the crack surface as in Fig. 9*d*,

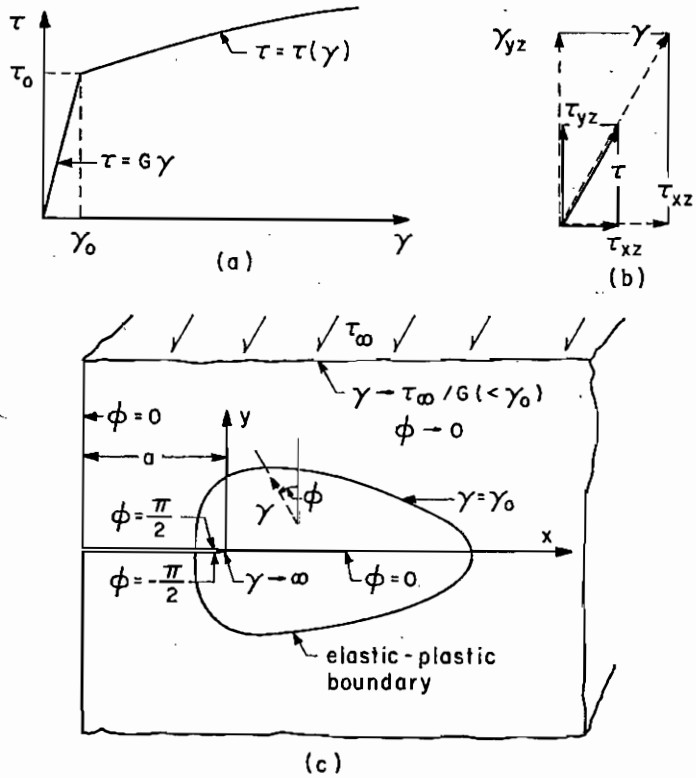

FIG. 10—(a *and* b) *Elastic-work hardening plastic anti-plane shear stress-strain relation, and* (c) *polar strain co-ordinate system* (γ *is magnitude of strain vector,* ϕ *is angle between strain vector and* y *axis*).

$$\left.\begin{aligned} \omega &= \frac{\pi K_{III}^2}{16\,\tau_o^2} \approx 0.196 \frac{K_{III}^2}{\tau_o^2} \\ u_o &= \frac{\gamma_o K_{III}^2}{4\tau_o^2} = \frac{4}{\pi} \gamma_o \omega \approx 1.272\, \gamma_o \omega \end{aligned}\right\} \quad \ldots\ldots\ldots\ldots (17c)$$

Comparing these last three results and Eq 13*a*, the particular shape of the yield surface is seen not to be of great influence in determining the extent of plasticity, in spite of the radically different plastic zones formed.

Neuber [*18*] first pointed out the possibility of obtaining anti-plane shear stress distributions in materials with nonlinear stress-strain relations of the elastic work-hardening plastic type. His results were limited to the "small scale yielding" case, in our present terminology, although this has unfortunately not been realized by some investigators (see the

subsequent discussion on stress concentrations due to smooth ended notches). Rice [9] provided a hardening anti-plane shear solution for sharp edge notches, including the finite crack configuration of Fig. 1 as a special case, through a procedure valid so long as the remotely applied shear stress τ_∞ does not exceed the initial yield stress τ_o, which marks the onset of plastic flow. These solutions are of the deformation plasticity type (that is, indistinguishable from nonlinear elastic solutions) rather than the physically appropriate incremental type. The principal shear stress and principal shear strain,

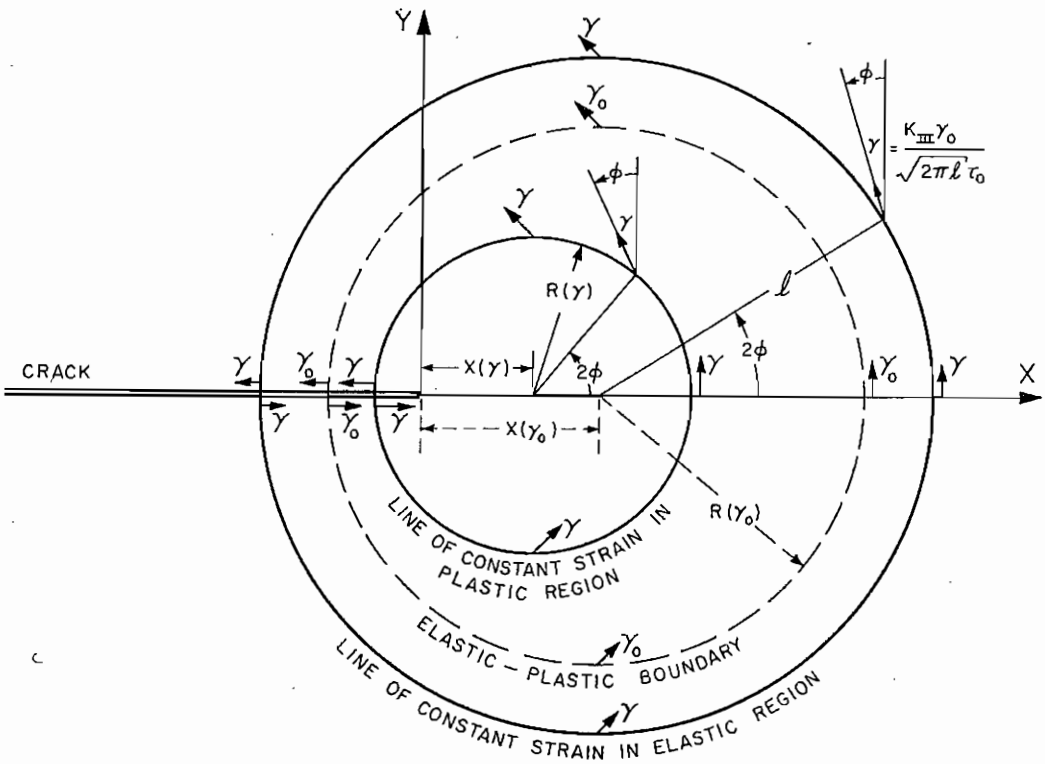

FIG. 11—*Geometry of small scale yielding near a crack tip for arbitrary relation between anti-plane shear stress and strain in the work hardening range.*

$$\tau = (\tau_{xz}^2 + \tau_{yz}^2)^{1/2}, \qquad \gamma = (\gamma_{xz}^2 + \gamma_{yz}^2)^{1/2} \ldots\ldots\ldots (18a)$$

are assumed uniquely related to one another by

$$\tau = G\gamma \quad \text{for} \quad \gamma < \gamma_o = \tau_o/G; \quad \tau = \tau(\gamma) \quad \text{for} \quad \gamma > \gamma_o \ldots . (18b)$$

where $\tau = \tau(\gamma)$ is the equation of the plastic portion of the stress strain curve (Fig. 10*a*). Component forms of the stress strain relations are

$$\tau_{xz} = \frac{\tau}{\gamma}\gamma_{xz}\,, \tau_{yz} = \frac{\tau}{\gamma}\gamma_{yz} \ldots\ldots\ldots\ldots\ldots (18c)$$

equivalent to assuming that the stress and strain vectors are colinear (Fig. 10*b*).

A polar strain coordinate system is employed (Fig. 10*c*) where γ is the magnitude of the strain vector and ϕ the angle between the strain vector and the y axis. Much as in the perfectly plastic case, physical coordinates x and y are related to derivatives of a potential function $\psi = \psi(\gamma, \phi)$ by [*9,18*]

$$x = -\sin\phi\,\frac{\partial\psi}{\partial\gamma} - \frac{\cos\phi}{\gamma}\,\frac{\partial\psi}{\partial\phi}, \quad y = \cos\phi\,\frac{\partial\psi}{\partial\gamma} - \frac{\sin\phi}{\gamma}\,\frac{\partial\psi}{\partial\phi} \quad \ldots(19a)$$

anti-plane displacements are

$$u_z = \gamma\,\frac{\partial\psi}{\partial\gamma} - \psi \quad \ldots(19b)$$

The potential function satisfies

$$\frac{\tau(\gamma)}{\gamma\tau'(\gamma)}\,\frac{\partial^2\psi}{\partial\gamma^2} + \frac{1}{\gamma}\,\frac{\partial\psi}{\partial\gamma} + \frac{1}{\gamma^2}\,\frac{\partial^2\psi}{\partial\phi^2} = 0 \quad \ldots(19c)$$

and appropriate boundary conditions may be set [*9*] as suggested by the labeling of Fig. 10*c*.

The small scale yielding solution views the crack as semi-infinite and imposes boundary conditions that the elastic inverse square root singularity (Eq 11*c*) be approached at large distances. In this case for $\gamma > \gamma_o$ (that is, for points in the plastic zone) the potential function is [*9,18*]

$$\psi = -\frac{\gamma_o K_{III}^2}{\tau_o}\,\gamma\sin\phi\int_\gamma^\infty \frac{du}{u^2\tau(u)} \quad (\gamma > \gamma_o) \quad \ldots(20)$$

A geometrical interpretation of this solution is given in Fig. 11. Upon introducing the functions of strain

$$\left.\begin{aligned} x(\gamma) &= \frac{K_{III}^2}{2\pi\tau_o^2}\left\{2\gamma_o\tau_o\int_\gamma^\infty \frac{du}{u^2\tau(u)} - \frac{\gamma_o\tau_o}{\gamma\tau(\gamma)}\right\} \\ R(\gamma) &= \frac{K_{III}^2}{2\pi\tau_o^2}\,\frac{\gamma_o\tau_o}{\gamma\tau(\gamma)} \end{aligned}\right\} \quad \ldots(21a)$$

physical coordinates are related to the strain vector and its orientation by

$$x = X(\gamma) + R(\gamma)\cos 2\phi, \qquad y = R(\gamma)\sin 2\phi \quad \ldots(21b)$$

As in Fig. 11, these require that lines of constant strain γ in the plastic region be circles of radius $R(\gamma)$ with center a distance $X(\gamma)$ ahead of the crack tip. The direction angle ϕ of the strain vector at any point on a constant strain circle is one half the angle made with the x axis by a line from the center of the circle to that point. Similarly, the elastic-plastic boundary is a circle with center at $X(\gamma_o)$ and radius $R(\gamma_o) = K_{III}^2/(2\pi\tau_o^2)$; this radius is independent of the form of the work hardening stress strain

curve. The plastic zone extends a distance $R(\gamma_o) + X(\gamma_o)$ ahead of the crack tip and $R(\gamma_o) - X(\gamma_o)$ behind the crack tip. From Eq 21*b*, since $\phi = 0$ on the line in front of the crack, distance x from the crack tip and strain $\gamma_{yz}(x, 0)$ are related by

$$x = \frac{\gamma_o K_{III}^2}{\pi\tau_o} \int_{\gamma_{yz}(x,0)}^{\infty} \frac{du}{u^2\tau(u)} \qquad (\gamma_{yz}(x, 0) > \gamma_o) \quad \ldots\ldots (22)$$

Stresses in the elastic region outside the circular plastic zone are given by

$$\tau_{yz} + i\tau_{xz} = \Omega(\zeta) = \frac{K_{III}}{\{2\pi[\zeta - X(\gamma_o)]\}^{1/2}} \quad \ldots\ldots\ldots (23)$$

so that, as noted earlier for the special case of perfect plasticity, the effect of yielding is to shift the elastic singularity stress distribution ahead a distance equal to that between the crack tip and center of the plastic zone. Lines of constant strain γ in the elastic region remain circular, but not concentric with the elastic plastic boundary (Fig. 11).

As an example, for a stress-strain relation following a power law

$$\tau = \tau_o(\gamma/\gamma_o)^N \qquad (\gamma > \gamma_o) \quad \ldots\ldots\ldots\ldots\ldots (24)$$

in the work hardening range,

$$R(\gamma) = \frac{1 + N}{1 - N} X(\gamma) = \frac{K_{III}^2}{2\pi\tau_o^2} (\gamma_o/\gamma)^{1+N} \quad \ldots\ldots\ldots (25a)$$

Thus the plastic zone extends a distance

$$\omega = R(\gamma_o) + X(\gamma_o) = \frac{1}{1 + N} \frac{K_{III}^2}{\pi\tau_o^2} \quad \ldots\ldots\ldots (25b)$$

ahead of the crack tip, and on the line ahead of the crack in the plastic region (Eq 22)

$$\gamma_{yz}(x, 0) = \gamma_o \left[\frac{K_{III}^2}{(1 + N)\pi\tau_o^2 x}\right]^{1/(1+N)} \quad \ldots\ldots\ldots (25c)$$

$$\tau_{yz}(x, 0) = \tau_o \left[\frac{K_{III}^2}{(1 + N)\pi\tau_o^2 x}\right]^{N/(1+N)} \quad \ldots\ldots\ldots (25d)$$

When the small scale yielding approximation is inappropriate, the solution for the potential function ψ (from which physical coordinates are obtained by Eq 19*a*) in the plastic region ($\gamma > \gamma_o$) takes the form [9]

$$\psi(\gamma, \phi) = \sum_{n=1}^{\infty} D_n f_n(\gamma) \sin[(2n - 1)\phi] \qquad (\gamma > \gamma_o) \quad \ldots\ldots (26a)$$

Here the set of functions $f_n(\gamma)$, $n = 1, 2, 3, \cdots$, satisfy the ordinary differential equations

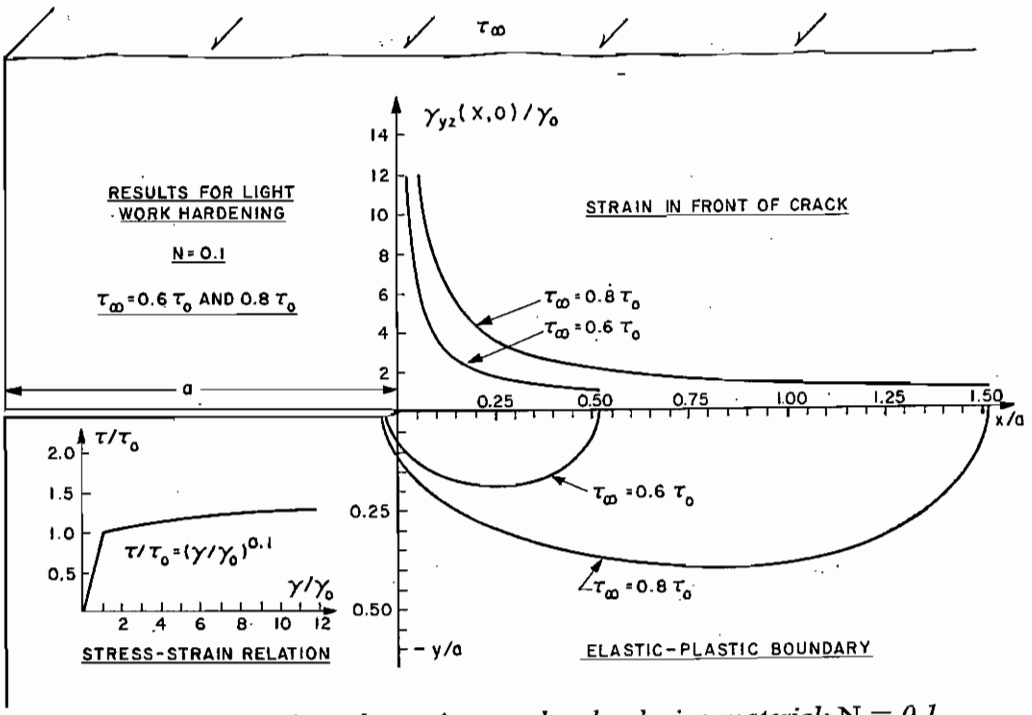

FIG. 12—*Anti-plane shear of power law hardening material;* N = *0.1.*

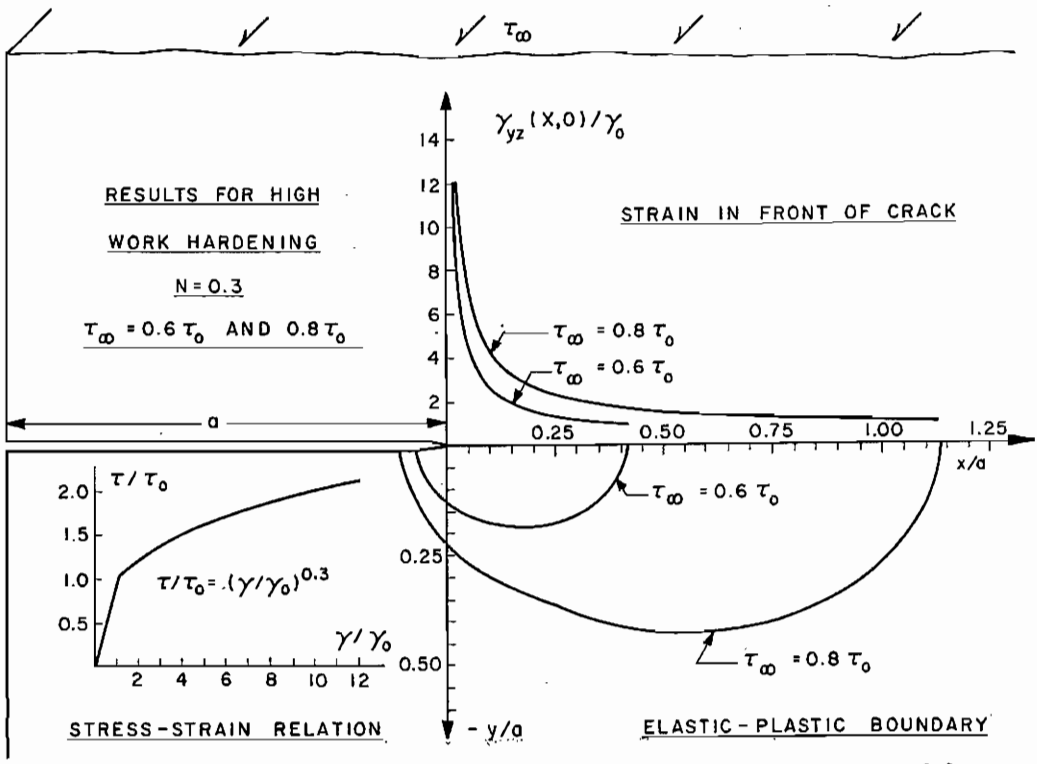

FIG. 13—*Anti-plane shear of power law hardening material;* N = *0.3.*

$$\frac{\tau(\gamma)}{\gamma\tau'(\gamma)} f_n''(\gamma) + \frac{1}{\gamma} f_n'(\gamma) - \frac{(2n-1)^2}{\gamma^2} f_n(\gamma) = 0 \ldots\ldots (26b)$$

with boundary conditions

$$f_n(\gamma_o) = 1, \qquad \lim_{\gamma\to\infty} f_n'(\gamma) = 0 \ldots\ldots\ldots\ldots (26c)$$

The set of coefficients D_n has been determined [9] for the edge crack configuration of Fig. 10*c* when the remotely applied stress is below the initial yield stress; they are linear in crack length and rather complicated functions of the form of the hardening stress-strain curve and the ratio of remotely applied stress to initial yield stress. Extensive numerical tabulations of the coefficients D_n have been published [9] for materials hardening according to the power law of Eq 24. Figures 12 and 13 show some of the final results in graphical form. In Fig. 12 the hardening

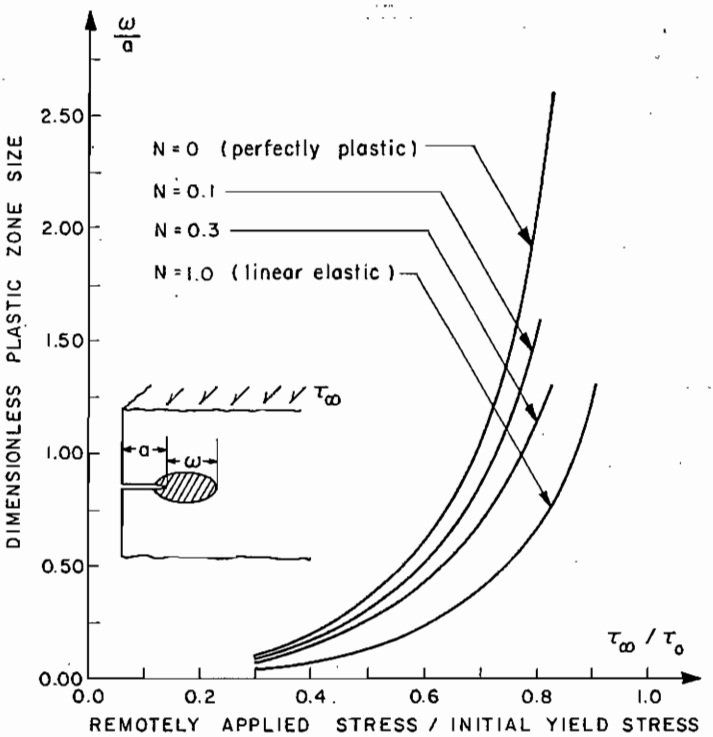

FIG. 14—*Plastic zone dimension as a function of net section stress and hardening exponent; anti-plane shear of material following* $\tau = \tau_0 (\gamma/\gamma_0)^N$ *in plastic range.*

exponent is $N = 0.1$; the position of the elastic plastic boundary (lower right quartile of figure) and strain distribution in the plastic region ahead of the crack tip (upper right quartile) are shown for $\tau_\infty = 0.6\ \tau_o$ and $\tau_\infty = 0.8\ \tau_o$. These remotely applied stress levels were chosen for illustration as they nicely typify the transition from the circular plastic zones of small scale yielding to the highly elongated plastic zone extending out to infinity as the remotely applied stress approaches the initial yield stress. The same results are graphed in Fig. 13 for a higher hardening exponent of $N = 0.3$.

The variation of plastic zone dimension ω with applied stress and hardening exponent N is shown in Fig. 14 for the edge crack of depth a in an infinite body of material hardening according to the power law of

Eq 24. At low stress levels the small scale yielding Eq 25*b* applies, with $K_{III} = \tau_\infty(\pi a)^{1/2}$. Significant deviations occur above about 30 per cent of the initial yield stress, the range for which the curves are drawn. The curve labeled $N = 0$ corresponds to perfect plasticity, and is simply Eq 14*a*. The other extreme, $N = 1.0$, corresponds to linear elastic behavior. Here the plastic zone dimension was computed directly from the elastic solution of Eq 7 by setting ω equal to the distance ahead of the crack tip at which $\tau_{yz}(x, 0) = \tau_o$, resulting in

$$\omega = a\{[1 - (\tau_\infty/\tau_o)^2]^{-1/2} - 1\} \qquad (N = 1.0) \ldots\ldots\ldots (27)$$

It is of interest to note that the relatively high hardening exponent of $N = 0.3$ gives a result about as close to the linear elastic prediction as to the perfectly plastic.

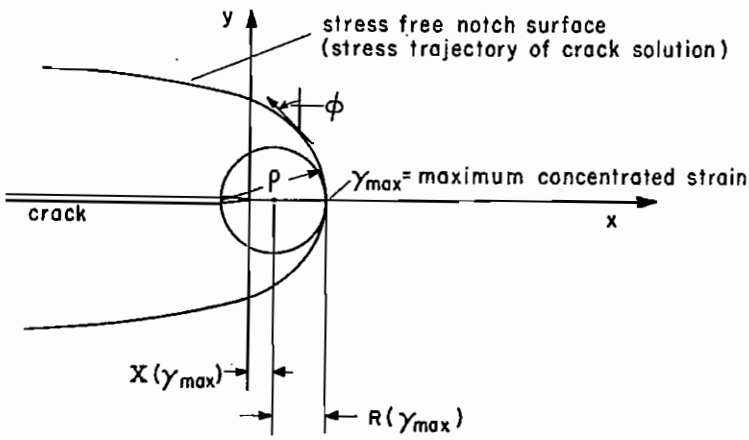

FIG. 15—*The anti-plane solution for a crack or sharp notch also provides a solution for a family of smooth ended notches.*

Neuber [*18*] has indicated that an anti-plane stress distribution for a crack or sharp ended notch also provides the stress distribution for a family of smooth ended notches. The stress free boundary condition is that the stress vector be tangent to the boundary. Thus the family of stress trajectories for, say, the crack solution is the family of corresponding smooth ended notches. From Eqs 19*a*, x and y are known as a function of γ and ϕ. Thus the stress trajectory equation (see Fig. 15)

$$dx + \tan\phi\, dy = 0 \ldots\ldots\ldots\ldots\ldots\ldots (28a)$$

becomes a differential equation for γ as a function of ϕ along a trajectory. Inserting initial conditions $\gamma = \gamma_{max}$ (maximum strain, occurring at notch tip) when $\phi = 0$, γ is determined as a function of ϕ and thus the x and y coordinates of points on the notch surface are determined as a function of ϕ. Upon solving for the radius of curvature ρ at the notch tip, one finds after some computations that

$$\rho = \left[\frac{\partial^2 \psi}{\partial \gamma \partial \phi} - \frac{1}{\gamma}\frac{\partial \psi}{\partial \phi}\right]_{\phi=0,\ \gamma=\gamma_{max}} \quad \ldots\ldots\ldots\ldots (28b)$$

For the small scale yielding solution, this turns out to be (Fig. 15)

$$\rho = 2R(\gamma_{max}) = \frac{K_{III}^2}{\pi \tau_o^2} \frac{\gamma_o \tau_o}{\gamma_{max} \tau(\gamma_{max})} \quad \ldots\ldots\ldots\ldots (29a)$$

Thus, defining $\tau_{max} = \tau(\gamma_{max})$ as the maximum concentrated strain, one finds Neuber's result [*18*] that for the family of smooth ended notches generated in the way described above and having the same root radius of curvature, the product of the maximum concentrated stress and strain is a constant independent of the stress-strain curve:

$$\gamma_{max}\tau_{max} = \frac{K_{III}^2}{\pi G \rho} \quad \ldots\ldots\ldots\ldots\ldots\ldots (29b)$$

Equivalently, the product of the stress and strain concentration factors has the same value as for the linear elastic case. Neuber unfortunately

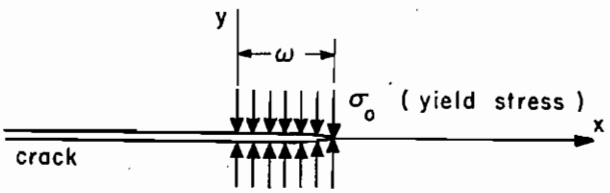

FIG. 16—*The effect of yielding is viewed as yield level stresses restraining an extended portion of the crack surface.*

failed to adequately emphasize the restriction of his result to what is here called the small scale yielding case; some investigators [*19,20*] have attempted to employ this result in the net section yielding range where it is incorrect. Rhee and McClintock [*21*] have pointed out that in the perfectly plastic case the family of stress free boundaries are circular arcs in the plastic region and

$$\gamma_{max}\tau_{max} = \left(\gamma_o \frac{\omega}{\rho}\right) \tau_o \quad \ldots\ldots\ldots\ldots\ldots\ldots (30a)$$

Were the Neuber result to hold at *all* stress levels, ω would have to be given always by the small scale yielding expression. We see from Fig. 6 that this is not the case, and indeed at 80 per cent of the limit stress Neuber's result (Eq 29*b*) is incorrect by a factor of about three for the edge notch in an infinite body. More generally, employing the solution of Eq 26*a* valid also at high stress levels, Eq 28*b* leads to

$$\rho = \sum_{n=1}^{\infty} (2n-1) D_n \left[f_n'(\gamma_{max}) - \frac{1}{\gamma_{max}} f_n(\gamma_{max})\right] \quad \ldots\ldots (30b)$$

for the relation between root radius and maximum concentrated strain.

Discrete Surfaces of Slip or Tensile Yielding

Several authors have proposed approximate treatments of crack tip plasticity based on a supposition that plastic flow is adequately modelled as either slip or tensile yielding on discrete surfaces emanating from the crack tip. Barenblatt [*22*] first considered models of this type, although his original application was to the influence of molecular "cohesive" forces on the form of deformation near a crack tip in brittle materials. Later Dugdale [*23*] replaced the cohesive forces of the Barenblatt theory with yield level stresses restraining the crack opening over an extended portion of the crack surface equal to the plastic zone dimension. Bilby, Cottrell, and Swinden [*24*] examined the same model but approached the mathematical problem from the point of view of a continuous array of dislocations distributed on a plane containing the crack and its yield zone. Further studies of models based on discrete surfaces of slip or tensile yielding have been made by Goodier and Field [*25*], Field [*26*], Smith [*27*], Rice [*7*], Keer and Mura [*28*], and Hahn and Rosenfield [*29*].

Figure 16 pictures the basic idea for the case of a discrete surface of tensile yielding ahead of the crack, as appropriate for the tensile mode. The influence of yielding is viewed as effectively extending the crack a distance ω ahead of its tip, with yield level stresses σ_o acting to restrain the extended crack surfaces. The computation is then entirely elastic, and the plastic zone size is determined as that length ω which makes the stresses bounded at the outer tip of the plastic zone. For the tensile mode, the small scale yielding solution which asymptotically approaches the crack tip elastic singularity leads to [*7*]

$$\omega = \frac{\pi}{8}\frac{K_I^2}{\sigma_o^2} \approx 0.392\frac{K_I^2}{\sigma_o^2} \qquad (31a)$$

The complex potentials from which stresses and displacements may be computed (Eq 5) are

$$\left.\begin{aligned} \Phi(\zeta) &= \frac{\sigma_o}{\pi}\arctan\left[\left(\frac{\omega}{\zeta-\omega}\right)^{1/2}\right] \\ \Psi(\zeta) &= \zeta\Phi'(\zeta) \end{aligned}\right\} \qquad (31b)$$

taking the branch cut along the crack line and plastic region, $-\infty < x < \omega$. Displacements $u_y(x, 0)$ of the extended crack surface in the plastic zone are given by [*7*]

$$u_y(x,0) = \frac{(\kappa+1)\sigma_o\omega}{2\pi G}\left\{\left(1-\frac{x}{\omega}\right)^{1/2} - \frac{1}{2}\frac{x}{\omega}\log\left[\frac{1+\left(1-\frac{x}{\omega}\right)^{1/2}}{1-\left(1-\frac{x}{\omega}\right)^{1/2}}\right]\right\} \qquad (31c)$$

$$0 < x < \omega,$$

and the crack opening displacement $u_y(0, 0) = u_o$ is

$$u_o = \frac{(\kappa + 1)\sigma_o\omega}{2\pi G} = \frac{(\kappa + 1)K_I^2}{16G\sigma_o} \quad \ldots\ldots\ldots\ldots (31d)$$

Here displacements are measured from zero along the crack line so that $2u_y(x, 0)$ is the total displacement between the upper and lower crack surfaces.

Similar results follow from the small scale yielding solution for in-plane shear. Replacing the tensile yield stress σ_o in Fig. 16 by a shear yield stress τ_o, the plastic zone size is

$$\omega = \frac{\pi}{8}\frac{K_{II}^2}{\tau_o^2} \quad \ldots\ldots\ldots\ldots\ldots\ldots\ldots (32a)$$

An equation identical to Eq 31*c* results for the sliding displacement $u_x(x, 0)$ in the plastic region, with σ_o replaced by τ_o and ω as above. The crack opening displacement $u_x(0, 0) = u_o$ is

$$u_o = \frac{(\kappa + 1)\tau_o\omega}{2\pi G} = \frac{(\kappa + 1)K_{II}^2}{16G\tau_o} \quad \ldots\ldots\ldots\ldots (32b)$$

Similarly for the case of anti-plane shear [*7*],

$$\omega = \frac{\pi}{8}\frac{K_{III}^2}{\tau_o^2} \quad \ldots\ldots\ldots\ldots\ldots\ldots\ldots (33a)$$

The sliding displacements $u_z(x, 0)$ in the plastic zone are again given by an equation identical to Eq 31*c*, but with the factor outside the bracket replaced by $4\tau_o\omega/\pi G$, and the crack opening displacement $u_z(0, 0) = u_o$ is

$$u_o = \frac{2\tau_o\omega}{\pi G} = \frac{K_{III}^2}{4G\tau_o} \quad \ldots\ldots\ldots\ldots\ldots\ldots (33b)$$

This solution is, of course, identical to that of Eqs 17*b* resulting from the highly anisotropic anti-plane shear yield surface of Fig. 9*c*. It is seen that anti-plane shear results, in this case, are also correct for in-plane shear if $1/G$ is replaced by $(\kappa + 1)/4G$ in the displacement formulae.

At high stress levels the small scale yielding solution is no longer useful and recourse must be made to complete solutions. For the finite crack of length $2a$ configuration of Fig. 1, subjected to a remotely applied tensile stress $(\sigma_y)_\infty = \sigma_\infty$, the resulting plastic zone size for discrete planes of tensile yielding at the ends of the crack is [*13–25*]

$$\omega = a\left[\sec\left(\frac{\pi\sigma_\infty}{2\sigma_o}\right) - 1\right] \quad \ldots\ldots\ldots\ldots\ldots (34a)$$

Identical formulas apply for in-plane or anti-plane shearing, with σ_∞/σ_o replaced by τ_∞/τ_o. The complex stress potentials (Eq 5) are

$$\left.\begin{aligned}\Phi(\zeta) &= \frac{\sigma_o}{\pi}\arctan\left[\left(\frac{\omega}{\zeta-\omega}\right)^{1/2}\left(\frac{2a+\omega}{\zeta+2a+\omega}\right)^{1/2}\left(\frac{\zeta+a}{a}\right)\right]-\frac{\sigma_\infty}{4}\\ \Psi(\zeta) &= -\zeta\Phi'(\zeta)+\frac{\sigma_\infty}{2}\end{aligned}\right\}\quad(34b)$$

For in-plane shear, σ_o is replaced by $-i\tau_o$ in the expression for $\Phi(\zeta)$ and the constant is replaced by $+i\tau_\infty/2$, and $\Psi(\zeta) = -2\Phi(\zeta) - \zeta\Phi'(\zeta) + i\tau_\infty$. The complex potential $\Omega(\zeta)$ for the anti-plane shear case is identical to the above expression for $\Phi(\zeta)$, but with σ_o replaced by $2\tau_o$ and the constant dropped. The crack opening displacement $u_y(0, 0) = u_o$ is

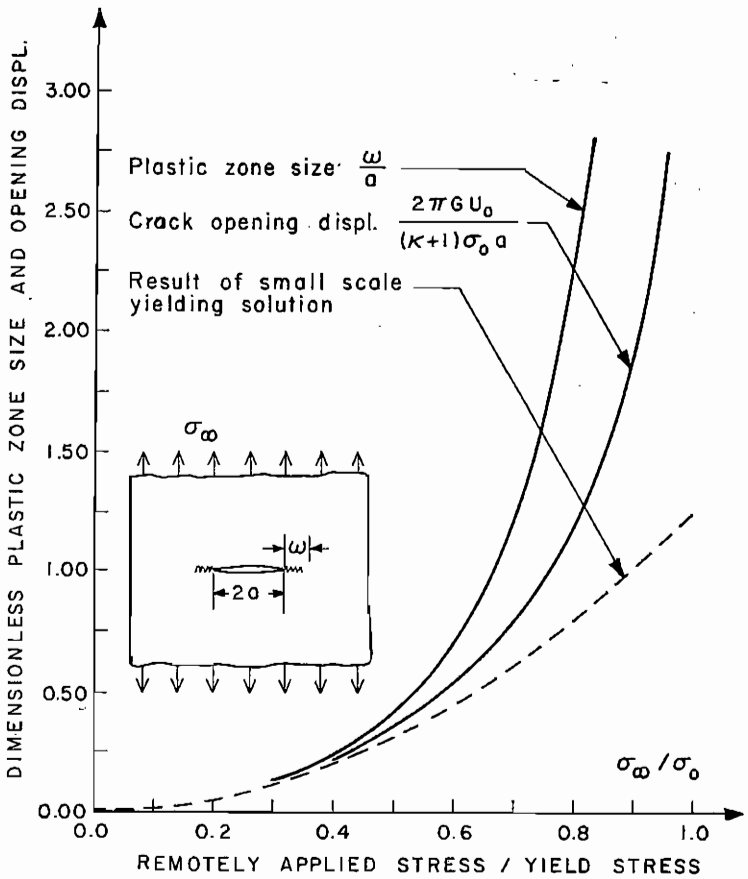

FIG. 17—*Plastic zone size and crack opening displacement as a function of applied stress; Discrete surfaces of tensile yielding at crack tips.*

$$u_o = \frac{(\kappa+1)\sigma_o a}{2\pi G}\log\left(1+\frac{\omega}{a}\right) = \frac{(\kappa+1)\sigma_o a}{2\pi G}\log\left[\sec\left(\frac{\pi\sigma_\infty}{2\sigma_o}\right)\right]\quad(34c)$$

Again, the same expression applies for in-plane or anti-plane shear with $1/G$ replacing $(\kappa+1)/4G$ in the latter case.

The plastic zone size and crack opening displacement given by the above expressions are graphed as a function of applied stress in Fig. 17. These appear in the dimensionless forms

$$\frac{\omega}{a} \text{ and } \frac{2\pi G u_o}{(\kappa + 1)\sigma_o a}$$

both of which equal $(\pi^2/8)\,(\sigma_\infty/\sigma_o)^2$ according to the small scale yielding solution of Eqs 31*a* and *d* upon noting that $K_I = \sigma_\infty(\pi a)^{1/2}$ in this case. The solid lines of Fig. 17 are Eqs 34*a* and *c* above; the dashed line is the result of the small scale yielding solution. As is similar to the anti-plane shear case of Figs. 6 and 7, the surrounding elastic singularity controls the plastic zone size up to about 30 to 40 per cent of the limit load, and the crack opening displacement up to about 40 to 50 per cent of the limit load.

The discrete surface of tensile yielding models for finite width planes with single edge, double edge, or central cracks are solved approximately by cutting appropriate segments from an infinite array of identical colin-

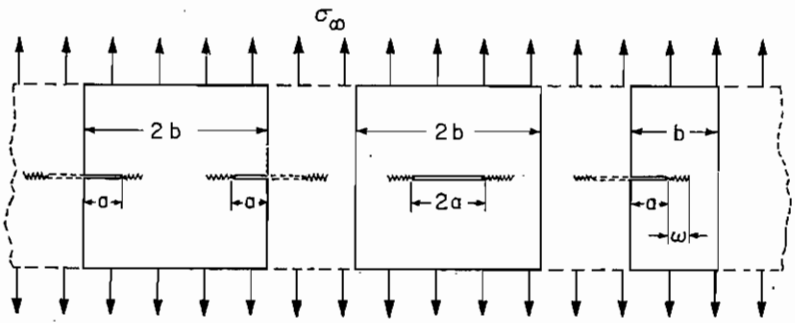

FIG. 18—*The infinite colinear array of identical cracks provides an approximate solution of the discrete surfaces of tensile yielding models for the double edge cracks, central crack, and single edge crack configurations.*

ear cracks, as in Fig. 18. The plastic zone size for this approximation is [*27*]

$$\omega = a\left\{\frac{2b}{\pi a}\arcsin\left[\sin\left(\frac{\pi a}{2b}\right)\sec\left(\frac{\pi\sigma_\infty}{2\sigma_o}\right)\right] - 1\right\} \quad \ldots\ldots (35a)$$

and the crack opening displacement is given by the integral

$$u_o = \frac{(\kappa + 1)\,\sigma_o b \sin\alpha}{2\pi^2 G}\int_\mu^{\pi/2} \frac{\cos\gamma}{(1 - \sin^2\alpha\sin^2\lambda)^{1/2}} \log \cdot\left[\frac{\sin(\lambda + \mu)}{\sin(\lambda - \mu)}\right] d\lambda \quad \ldots (35b)$$

where $\alpha = \pi(a + \omega)/(2b)$ and $\mu = (1 - \sigma_\infty/\sigma_o)\pi/2$. Numerical results have been given by Bilby and Swinden [*30*]. Noting that the stress intensity factor is

$$K_I = \sigma_\infty(\pi a)^{1/2}\left[\frac{2b}{\pi a}\tan\left(\frac{\pi a}{2b}\right)\right]^{1/2} \quad \ldots\ldots\ldots\ldots (35c)$$

for the infinite array, these results may be shown to reduce to the small scale yielding solution at low stress levels. The plasticity models for the single edge, double edge, and central crack configurations, as based on the infinite array, are likely accurate to about the same order that the elastic stress intensity factors are given by the infinite array expression (Eq 35*c*). From the discussion of Paris and Sih [*4*], the approximation would be best for short central cracks and worse for single edge cracks due to bending in the latter case. In fact, the limit load is even given incorrectly in the single edge crack case as some compressive yielding must occur to offset the bending induced by the lack of symmetry. Smith [*27*] has discussed the discrete surfaces of yielding model for other configurations involving more than one crack; Rice [*7*] has given general methods through which plasticity solutions may be determined directly

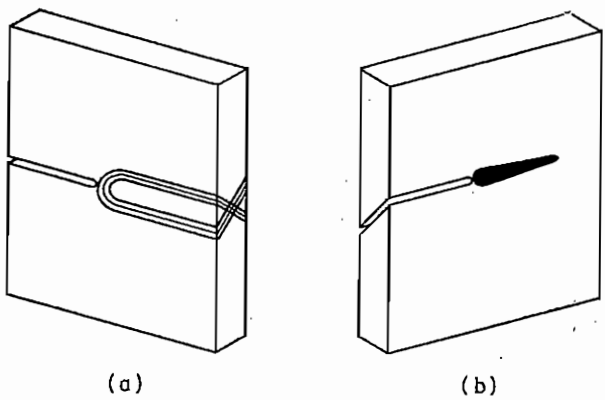

FIG. 19—*Plane stress plasticity in thin sheet may be modeled as discrete surface of tensile yielding at crack tip:* (a) *two 45 deg slip bands ahead of crack and* (b) *fully developed 45 deg shear lip crack with one slip band.*

from known elastic solutions for single cracks in infinite bodies, and has given the detailed solution for wedge forces on a crack surface.

Hahn and Rosenfield [*29*] have discussed the particular relevance of the discrete surface of tensile yielding model for plane stress plasticity. As in Fig. 19*a*, plastic flow ahead of flat through-the-thickness cracks in thin sheets tends to consist of two intersecting 45-deg shear bands. The plasticity is then localized to a narrow region of height roughly equal to the sheet thickness. Presumably for an inclined 45-deg crack (Fig. 19*b*) as may occur after a plane stress transition in fatigue, a single narrow 45-deg shear band would appear ahead of the crack. The average plastic extensional strain, $\bar{\epsilon}_y^p$, would equal $2u_y(x, 0)/t$ in either case, where t is the sheet thickness and $u_y(x, 0)$ the displacements calculated from the discrete surface of tensile yielding model. A plane stress analysis based on digital computer solutions of the governing elastic-plastic equations has recently been presented by Swedlow, Williams, and Yang [*36*]. While their formulation was two-dimensional and thus

naturally does not reflect the inclined 45-deg shear band patterns observed in steels [*29*,*37*], their techniques show the promise of highly accurate numerical solutions to configurations such as cracked bodies exhibiting steep stress and strain gradients. Details of the deformation very near the crack tip remain obscure. Approximate methods of determining the plane stress distributions near cracks, based on photoelastic analyses, have been proposed by Dixon and Strannigan [*38*].

Keer and Mura [*28*] treated the penny shaped crack of radius a in an infinite solid subjected to the uniform remote tension σ_∞, employing the model of a discrete annular surface of tensile yielding surrounding the crack. In this case the plastic zone size is given by

$$\omega = a\{[1 - (\sigma_\infty/\sigma_o)^2]^{-1/2} - 1\} \quad \ldots\ldots\ldots\ldots (36a)$$

and the crack opening displacement by

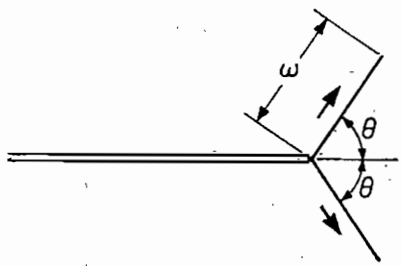

FIG. 20—*Discrete in-plane slip lines near crack under tension; plane strain mode of yielding.*

$$u_o = \frac{2(1-\nu)\sigma_o\omega}{\pi G(1+\omega/a)} = \frac{2(1-\nu)\sigma_o a}{\pi G}\{1 - [1 - (\sigma_\infty/\sigma_o)^2]^{1/2}\} \quad \ldots (36b)$$

It is of interest to note that for the penny shaped crack, the crack opening displacement approaches a finite limit as the remotely applied stress approaches the limit value, $\sigma_\infty = \sigma_o$. Since $K_I = 2\sigma_\infty(a/\pi)^{1/2}$ for the penny shaped crack [*4*], both ω and u_o may being shown to take the form of the small scale yielding results (Eqs 31*a* and *d*) at low stress levels (provided the plane strain value of $\kappa = 3 - 4\nu$ is chosen), even though these were derived for the planar case.

A model for tensile deformation near a crack tip, by in-plane sliding on two discrete slip surfaces inclined at angles $\pm\theta$ with the crack line, is pictured in Fig. 20. As has been seen in the last section, such plasticity distributions constitute an exact solution for anti-plane shearing of materials with single crystalline yield surfaces. Whether analogous results occur in the tensile case is currently unknown; however, such discrete slip models may be useful in determining gross features of plane strain yielding, just as the discrete surface of tensile yielding is useful for the plane stress situations. An exact method of solution would be to determine the stresses due to the application of external loads and yield level

shear stresses τ_o along the slip lines, imposing also the condition of zero normal displacement discontinuity, and then to choose the slip line length so that stresses are bounded at the outer tips of the slip lines. The mathematical difficulties are considerable and therefore an approximate solution is given based on the in-plane shear results of Eqs 32*a* and *b*.

Employing the singular terms of the complex potentials (Eq 11*a*) and Eqs 5, the elastic singularity gives the shear stress

$$\tau_{r\theta} = \tfrac{1}{2}K_{\mathrm{I}} \sin\theta \cos(\theta/2)\,(2\pi r)^{-1/2} \quad \ldots\ldots\ldots\ldots (37a)$$

along the prospective slip line. Now Eq 32*a* gives the slip line length required to relax a shear stress $K_{\mathrm{II}}(2\pi r)^{-1/2}$. It is plausible to assume that the inclined slip line length in Fig. 20 required to relax the shear stress of Eq 37*a* is given approximately by the same expression, but with K_{II} replaced by $\tfrac{1}{2}K_{\mathrm{I}} \sin\theta \cos(\theta/2)$. Thus

$$\omega \approx \frac{\pi K_{\mathrm{I}}^2 \sin^2\theta \cos^2(\theta/2)}{32\tau_o^2} \quad \ldots\ldots\ldots\ldots (37b)$$

is the length of a slip line inclined at angle θ. It is also plausible to assume that each slip line produces a total slip displacement jump twice the crack opening displacement given by Eq 32*b* (recall that for a slip line ahead of the crack, the opening displacement is one half the total displacement discontinuity), so that the slip opening displacement u_o produced by sliding along each of the two slip lines is given approximately by

$$u_o \approx \frac{(\kappa+1)\tau_o\omega}{\pi G} \approx \frac{(\kappa+1)K_{\mathrm{I}}^2 \sin^2\theta \cos^2(\theta/2)}{32G\tau_o} \quad \ldots\ldots (37c)$$

While these approximations may appear somewhat arbitrary, it is interesting to note that should results for a slip line ahead of the crack be similarly employed to approximate the inclined slip line cases in antiplane shear, the plastic zone size and opening displacement of Eqs 17*c* for the 90-deg slip lines (Fig. 9*d*) would be given exactly, and for the 45-deg slip lines (Fig. 9*b*) the zone size and opening displacement of Eqs 17*a* would be given to within the errors of about 4 and 40 per cent, respectively.

If θ is taken as 90 deg in the above equations, the yield stress in shear set equal to one half the yield stress in tension and the plane strain value of κ chosen with a Poisson ratio of 0.3, one obtains for plane strain conditions

$$\omega \approx 0.196\frac{K_{\mathrm{I}}^2}{\sigma_o^2},\ u_o \approx 0.225\frac{K_{\mathrm{I}}^2}{E\sigma_o} \text{ (plane strain)} \quad \ldots\ldots (38a)$$

Here $E = 2(1+\nu)G$ is Young's modulus. The values when $\theta = 45$ deg

are about 15 per cent lower. For comparison, using Eqs 31*a* and *d* as descriptive of plane stress conditions,

$$\omega \approx 0.392 \frac{K_I^2}{\sigma_o^2},\ u_o \approx 0.500 \frac{K_I^2}{E\sigma_o} \text{ (plane stress)} \ldots\ldots\ldots (38b)$$

These results suggest that in the small scale yielding range, the maximum plastic zone dimension and crack opening displacement are roughly half as large for plane strain conditions as compared to plane stress condi-

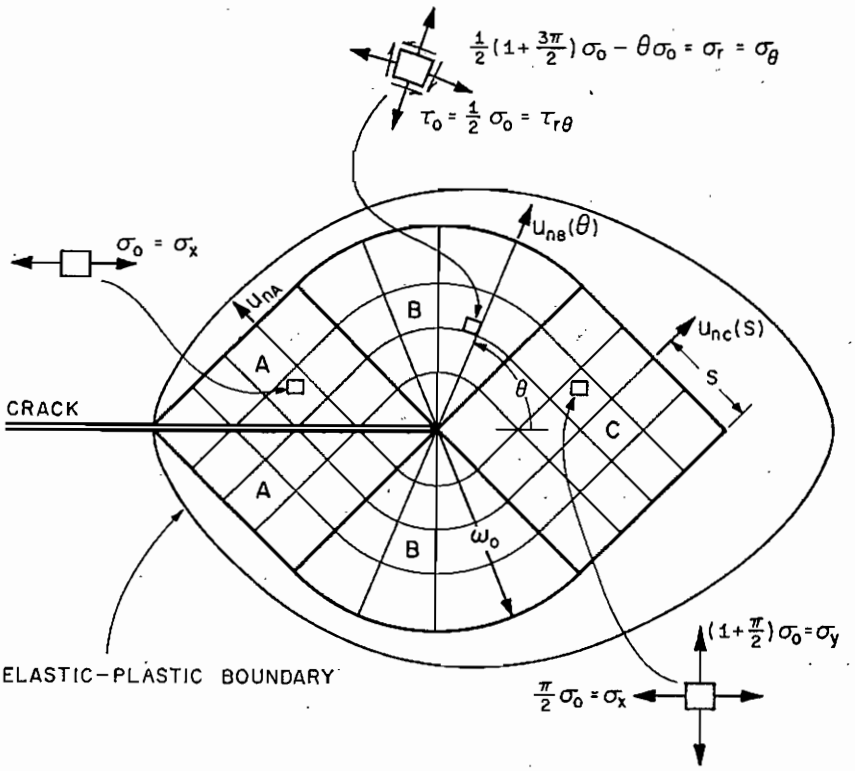

FIG. 21—*Slip line field immersed in plane strain plastic zone surrounding crack tip; constant stress regions joined by centered fans.*

tions. Another approach to plane strain yielding is considered in the next section. While one generally anticipates that plane strain plastic yielding will produce a "spread out" plastic region, a discrete slip line model may be particularly appropriate for unstable materials exhibiting upper and lower yield points.

Plane Strain Slip Line Field

While models based on discrete surfaces of slip or tensile yielding give at best gross features of tensile plasticity, some of the detailed features of plane strain yielding can be studied through recourse to the slip line theory [*13,31*]. F. A. McClintock has recently shown the author some yet unpublished experimental results on yielding in doubly edge notched

steel bars. Long bars with side grooves were compressed and later sectioned in the center where plane strain conditions should prevail. Etching revealed that the plastic region completely surrounded the crack tip, much as in Fig. 21. At what *appears* to be a transition to limit conditions at high stress levels, a few discrete slip lines inclined at roughly 45 deg to the crack line (as in Fig. 20 with $\theta = 45$ deg) shoot out from the smooth plastic region of Fig. 21.

The plane strain plastic slip line theory is exact only when Poisson's ratio is ½ or when plastic strains are much larger than elastic strains [*31*]. Neither of these conditions are met exactly; nevertheless, we proceed to examine the stress and strain distribution near the crack tip on the basis of this theory. The stress free boundary conditions on the crack surface determine the entire stress fields in the largest isosceles right triangles, labeled A in Fig. 21, which may be fit in the plastic zone. The stresses are constant in regions A and

$$\sigma_x = \sigma_o, \qquad \sigma_y = \tau_{xy} = 0 \qquad \text{(region } A\text{)} \ldots\ldots\ldots (39a)$$

Now any slip line emanating in region A, and finding its way to the line in front of the crack, must cross that line at 45 deg. Thus, the same hydrostatic stress buildup [*13*] occurs on each slip line, so that stresses are constant on the line ahead of the crack. Therefore, another constant stress region C is determined ahead of the crack, and in this region

$$\sigma_x = \frac{\pi}{2}\sigma_o, \qquad \sigma_y = \left(1 + \frac{\pi}{2}\right)\sigma_o, \qquad \tau_{xy} = 0 \qquad \text{(region } C\text{)} \ldots (39b)$$

$\pi\sigma_o/2$ being the hydrostatic stress buildup in excess of the tensile yield strength. Centered fans, regions B of Fig. 21, must join such constant state regions, and employing polar coordinates the stresses in the upper fan are [*13*]

$$\sigma_r = \sigma_\theta = \frac{1}{2}\left(1 + \frac{\pi}{2}\right)\sigma_o - \theta\sigma_o, \; \tau_{r\theta} = \tau_o = \frac{1}{2}\sigma_o \qquad \text{(region } B\text{)} \ldots (39c)$$

Making the assumption of incompressible elastic behavior ($\nu = ½$), strain and displacement distribution in the slip line net may be worked out in terms of displacements on the outer boundary of the three regions. Once the normal displacements u_n are specified at each point of the outer boundary, the interior strain and displacement fields are determined. Alternately, such a slip line net permits the arbitrary specification of only the normal displacements. Letting $u_{nc}(s)$ be displacements in the normal direction on the boundary of region C, with s measured as shown in Fig. 21, employing symmetry restrictions and following the treatment of Prager and Hodge [*13*], displacements in region C are

$$\left.\begin{aligned} u_x &= \frac{1}{\sqrt{2}}\left[u_{nC}\left(\omega_o - \frac{x-y}{\sqrt{2}}\right) + u_{nC}\left(\omega_o - \frac{x+y}{\sqrt{2}}\right)\right] \\ u_y &= \frac{1}{\sqrt{2}}\left[u_{nC}\left(\omega_o - \frac{x-y}{\sqrt{2}}\right) - u_{nC}\left(\omega_o - \frac{x+y}{\sqrt{2}}\right)\right] \end{aligned}\right\} \quad \ldots(40a)$$

where ω_o is the radius of the centered fans. Differentiating to obtain strains,

$$\left.\begin{aligned} \epsilon_y &= -\epsilon_x = \frac{1}{2}\left[u'_{nC}\left(\omega_o - \frac{x-y}{\sqrt{2}}\right) + u'_{nC}\left(\omega_o - \frac{x+y}{\sqrt{2}}\right)\right] \\ \gamma_{xy} &= 0 \end{aligned}\right\} \quad \ldots(40b)$$

Setting $y = 0$, the strain $\epsilon_y(x,0)$ along the line ahead of the crack is

$$\epsilon_y(x,0) = u'_{nC}(\omega_o - x/\sqrt{2}) \quad \ldots(40c)$$

The extensional strain at distance x ahead of the crack tip is the derivative of normal displacement with respect to arc length on the outer boundary evaluated at $s = \omega_o - x/\sqrt{2}$. Note that no singularity occurs as the crack tip is approached along the line ahead of the crack. Letting $u_{nB}(\theta)$ be normal displacements along the outer boundary of the centered fans and imposing continuity conditions along the common boundary of B and C, displacements in the fan region B are

$$\left.\begin{aligned} u_r &= u_{nB}(\theta) \\ u_\theta &= -\int_{\pi/4}^{\theta} u_{nB}(\psi)\, d\psi - u_{nC}(\omega_o - r) \end{aligned}\right\} \quad \ldots(41a)$$

The corresponding strain field in the centered fan is

$$\left.\begin{aligned} \epsilon_r &= \epsilon_\theta = 0 \\ \gamma_{r\theta} &= \frac{1}{r}\left[u'_{nB}(\theta) + \int_{\pi/4}^{\theta} u_{nB}(\psi)\, d\psi + u_{nC}(\omega_o - r)\right] \\ &\qquad + u'_{nC}(\omega_o - r) \end{aligned}\right\} \quad \ldots(41b)$$

Just as in the anti-plane shear case, the centered fan focuses a $1/r$ shear strain singularity into the crack tip, but now the focusing is from above and below rather than from in front of the crack tip.

While the general features of the plane strain yielding are qualitatively clear, further work remains to be done before quantitative results are developed. Studies are currently underway on the matching of a slip line net with the surrounding elastic field so that the dimension ω_o and normal displacements of the outer boundary may be estimated. Several questions remain. The assumption of elastic incompressibility is unrealistic, and since plastic strains are clearly not enormous in comparison

to elastic strains in regions A and C, some perturbation of the above solution will occur due to plastic flow in the z direction. Further, it is presently unclear as to whether the slip line net of Fig. 21 occupies a major portion of the plastic region or a small fraction, and also as to whether the discrete slip lines alluded to earlier constitute simply a transition to large scale yielding or an intrinsic part of the yielding even at low stress levels.

The large stresses generated in front of a crack under plane strain conditions likely extend to high applied stress levels, the regime in which yielding is controlled by the elastic singularity. This would be consistent with the greater success of elastic fracture mechanics for plane strain failures [*14*]. Judging from the limit analysis solutions summarized by Drucker [*32*] and McClintock [*33*], at applied stress levels causing net section yielding the stress and strain distributions near the crack tip are strongly dependent on geometry; the double edge notch configuration permits the persistence of hydrostatic stress buildup, whereas the single edge notch and central configurations do not.

Part II Mechanics of Fatigue Crack Propagation

The elastic-plastic mechanics developed in Part I is applied to fatigue crack propagation in this part of the paper. Solutions of the various models for unloading and cyclic loadings are given, and parameters which may rationally be expected important in fatigue crack propagation are identified. Theories of crack growth, seeking to relate cyclic crack tip plasticity to microstructural "damage" accumulation and material separation, are critically surveyed in the light of experimental results and general consistency with the elastic-plastic analyses.

Elastic-Plastic Response to Cyclic Loadings

All of the elastic-perfectly plastic models discussed in Part I have the common feature of involving proportional plastic flow; components of the plastic strain tensor (or displacement discontinuity components where discrete surfaces of slip or yielding are involved) remain in constant proportion to one another at each point of the plastic region. This permits a general treatment of the response to unloading, reloading, and cyclic loading through the plastic superposition method developed in special cases by Hult and McClintock [*15*] and Rice [*7*]. Undoubtedly, the persistence of proportional flow is much more a commentary on our mathematical ingenuity than on the physical situation. Compressibility effects in plane strain yielding as well as the transition from in-plane deformation to inclined 45-deg shear bands in plane stress yielding constitute deviations from proportional flow; these may, nevertheless, be expected insignificant for large plane strains and well developed plane stress yielding.

Suppose a cracked body is loaded by a system of stresses proportional to some parameter L, and that the loading parameter is reduced by an amount ΔL to a lower level $L - \Delta L$. To the extent that crack tip rounding by plastic deformation is neglected, the stress concentration factor is effectively infinite, and reverse plastic flow commences with the first increment of load reduction, creating a new plastic zone of reversed deformation imbedded in the plastic zone accompanying the original

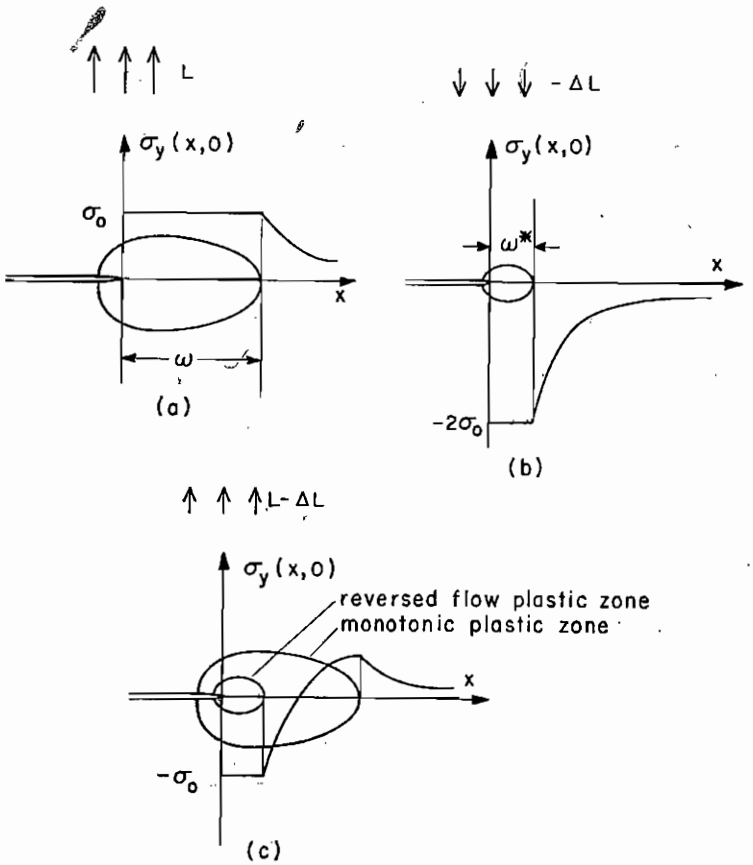

FIG. 22—*Plastic superposition for unloading. Adding* (b) *for load* $-\Delta$L *with a doubled yield stress to* (a) *gives the solution* (c) *resulting after unloading from* L *to* L-ΔL. *Reloading,* L-ΔL *to* L, *restores* (a).

loading (Fig. 22). When flow is proportional, the effect of unloading is to reverse the direction of stresses in the reversed flow region, without otherwise affecting their magnitude or distribution. The changes in stresses, strains, and displacements due to load reduction are then given by a solution identical to that for original monotonic loading, but with the loading parameter replaced by the load reduction ΔL and the yield strain and stress replaced by *twice* their values for original loading, so that stresses have the correct magnitude and direction in the reversed zone when the changes due to load reduction are subtracted from the distributions corresponding to the original monotonic loading. The procedure is illustrated in Fig. 22. Neglecting the possibility of crack closure,

the plastic superposition is valid up to the point where the reversed plastic zone is equal in size to the original plastic zone accompanying monotonic loading, which corresponds to complete load reversal ($\Delta L = 2L$). Crack closure always intervenes before complete load reversal, as discussed subsequently. For unloadings L to $L - \Delta L$, reloadings $L - \Delta L$ to L, and subsequent load cycles which do not cause crack closure, the reversed plastic zone size and cyclic variations in stresses, strains, and displacements depend *only* on the load fluctuation ΔL and are independent of the maximum load L.

As an example, for the finite crack in a large body configuration of Fig. 1, stress, strain, and displacement results from the elastic-perfectly plastic models considered in Part I may be generally represented in the form

$$\left.\begin{aligned} \sigma_{ij} &= \sigma_o \textstyle\sum_{ij}(r/a, \theta, \sigma_\infty/\sigma_o) \\ \epsilon_{ij} &= \epsilon_o E_{ij}(r/a, \theta, \sigma_\infty/\sigma_o) \\ u_i &= \epsilon_o a U_i(r/a, \theta, \sigma_\infty/\sigma_o) \end{aligned}\right\} \quad \ldots\ldots\ldots\ldots\ldots (42a)$$

for monotonic loadings, where r, θ are polar coordinates centered at the crack tip, σ_∞ is a remotely applied stress (shear or tension), σ_o and ϵ_o are a representative yield stress and strain, and $\sum_{ij}$, E_{ij}, and U_i are dimensionless functions of their arguments, reversing sign with sign reversals of σ_∞. The distance ω to the elastic-plastic boundary along any radial line at angle θ may be represented as

$$\omega = a\rho(\theta, \sigma_\infty/\sigma_o) \quad \ldots\ldots\ldots\ldots\ldots\ldots\ldots (42b)$$

Now if the applied stress is reduced in magnitude by $\Delta\sigma_\infty$, the above formulas apply for the changes in stress, strain, and displacement, as well as for the position of the reversed plastic region boundary, provided σ_∞ is replaced by $\Delta\sigma_\infty$ and σ_o, ϵ_o replaced by $2\sigma_o$, $2\epsilon_o$. Thus the distance ω^* to the reversed flow region boundary along any radial line at angle θ is

$$\omega^* = a\rho(\theta, \Delta\sigma_\infty/2\sigma_o) \quad \ldots\ldots\ldots\ldots\ldots\ldots\ldots (43a)$$

The stress, strain, and displacement after unloading are $\sigma_{ij} - \Delta\sigma_{ij}$, $\epsilon_{ij} - \Delta\epsilon_{ij}$, $u_i - \Delta u_i$, where the variations due to load reduction from σ_∞ to $\sigma_\infty - \Delta\sigma_\infty$ are

$$\left.\begin{aligned} \Delta\sigma_{ij} &= 2\sigma_o \textstyle\sum_{ij}(r/a, \theta, \Delta\sigma_\infty/2\sigma_o) \\ \Delta\epsilon_{ij} &= 2\epsilon_o E_{ij}(r/a, \theta, \Delta\sigma_\infty/2\sigma_o) \\ \Delta u_i &= 2\epsilon_o a U_i(r/a, \theta, \Delta\sigma_\infty/2\sigma_o) \end{aligned}\right\} \quad \ldots\ldots\ldots\ldots (43b)$$

Complete load removal ($\Delta\sigma_\infty = \sigma_\infty$) leaves residual stresses and displacements; from Eqs 42 and 43, their values are those at full load σ_∞

minus twice those at half load $\sigma_\infty/2$. Reloading, $\sigma_\infty - \Delta\sigma_\infty$ to σ_∞, restores stresses, strains, and displacements to values taken before unloading. Cycling over a stress range $\Delta\sigma_\infty$ produces alterations $\Delta\sigma_{ij}$, $\Delta\epsilon_{ij}$, and Δu_i with each load rise and fall as given by Eqs 43*b*, with Eq 43*a* giving ω^*, the size of the zone of cyclic plasticity.

The small scale yielding range is doubled for cyclic loadings since σ_∞/σ_o is now replaced by $\Delta\sigma_\infty/2\sigma_o$. Thus if the elastic stress intensity factor is found to control some aspect of the plasticity up to a certain per cent of the limit load, the cyclic variation in elastic stress intensity factor controls the corresponding cyclic aspect of the plasticity up to load variations which are double that per cent of the limit load

The maximum plastic zone dimension and crack opening displacement have been plotted in Figs. 6 and 7 for anti-plane shearing of a Tresca-Mises material and in Fig. 17 for a discrete surface of tensile yielding (or, with appropriate substitutions, slip) ahead of the crack. The same figures apply for load cycling with ω replaced by ω^*, u_o replaced by $\Delta u_o/2$, and τ_∞ (or σ_∞) replaced by $\Delta\tau_\infty/2$ (or $\Delta\sigma_\infty/2$). Taking from these figures 40 per cent of the fully plastic load as the upper limit on the small scale yielding range, the corresponding upper limit on the small scale yielding range for load cycling extends to load variations which are 80 per cent of the limit load. Thus, for example, in a tension-tension cyclic loading with a maximum stress $\sigma_\infty = 0.8\ \sigma_o$, the total plastic flow is poorly described by the Irwin stress intensity factor, while the embedded cyclic plastic flow is determined to within a small error by the variation in the stress intensity factor.

Small scale yielding solutions for load cycling are obtained directly from those for monotonic loading by replacing the stress intensity factor by its variation and doubling the yield stress and strain. Thus, for example, in the anti-plane shear of a Tresca-Mises material one obtains from the monotonic loading solutions of Eqs 12 and 13

$$\left.\begin{aligned} \omega^* &= \frac{(\Delta K_{III})^2}{4\pi\tau_o^2}\left(\omega = \frac{K_{III}^2}{\pi\tau_o^2}\right) \\ \Delta\gamma_{yz}(x,0) &= 2\gamma_o\frac{\omega^*}{x}\left(\gamma_{yz}(x,0) = \gamma_o\frac{\omega}{x}\right) \\ \Delta u_o &= 2\gamma_o\omega^* = \frac{\gamma_o(\Delta K_{III})^2}{2\pi\tau_o^2}\left(u_o = \gamma_o\omega = \frac{\gamma_o K_{III}^2}{\pi\tau_o^2}\right) \end{aligned}\right\} \quad \ldots\ldots(44)$$

for the cyclic plastic zone dimension, cyclic strain variation ahead of the crack tip in the cyclic plastic zone, and cyclic variation in crack opening displacement. Similarly, for a discrete surface of tensile yielding one obtains from Eqs 31

$$\left.\begin{aligned} \omega^* &= \frac{\pi(\Delta K_I)^2}{32\sigma_o^2} \qquad \left(\omega = \frac{\pi K_I^2}{8\sigma_o^2}\right) \\ \Delta u_o &= \frac{(\kappa+1)\sigma_o\omega^*}{\pi G} = \frac{(\kappa+1)(\Delta K_I)^2}{32G\sigma_o} \\ \left(u_o = \frac{(\kappa+1)\sigma_o\omega}{2\pi G}\right. &= \left.\frac{(\kappa+1)K_I^2}{16G\sigma_o}\right) \end{aligned}\right\} \quad \ldots\ldots\ldots (45)$$

In these two examples, as for all perfectly plastic small scale yielding situations, a cyclic variation in the stress intensity factor from zero to some maximum value results in a cyclic plastic zone of reversing deformation one quarter the maximum plastic zone size, and a variation in crack opening displacement over one half the total opening.

Since a residual displacement remains at the crack tip after load removal, the crack surfaces remain propped apart by the plastic flow. A rough estimate of the stress variation required to initiate contact of the crack surfaces may be had by examining the anti-plane shear case. Cracks do not open or close in this case, but rather slide. However, the load variation at which the shear displacement jump returns to zero at the crack midpoint of Fig. 1 should give a good estimate of the tensile load variation required to initiate closure. Supposing plastic flow to give the crack an effective length of $2l(>2a)$, from the elasticity solution of Eq 7 displacements along the upper crack surface are

$$u_z(x,0) = \frac{\tau_\infty}{G}[l^2 - (x+a)^2]^{1/2} \quad \ldots\ldots\ldots\ldots (46a)$$

Choosing l to give the small scale yielding crack opening displacement result of Eq 13, which is noted from Fig. 7 to be fairly accurate up to about 60 to 70 per cent of the limit load,

$$l = a[1 + (\tau_\infty/\tau_o)^2]^{1/2} \quad \ldots\ldots\ldots\ldots\ldots\ldots (46b)$$

At low stress levels this agrees with the interpretation of considering the crack to be longer by half the plastic zone size. The change in displacements of the crack surface due to a load reduction $\Delta\tau_\infty$ is then

$$\Delta u_z(x,0) = \frac{\Delta\tau_\infty}{G}[(l^*)^2 - (x+a)^2]^{1/2} \quad \ldots\ldots\ldots\ldots (46c)$$

where

$$l^* = a[1 + (\Delta\tau_\infty/2\tau_o)^2]^{1/2} \quad \ldots\ldots\ldots\ldots\ldots\ldots (46d)$$

Setting $\Delta u_z = u_z$ at the crack midpoint $x = -a$, one finds that closure initiates at a stress reversal satisfying

$$\left(\frac{\Delta\tau_\infty}{\tau_\infty}\right)^2 = 2\left(\frac{\tau_o}{\tau_\infty}\right)^2\left\{\left[1 + \left(\frac{\tau_\infty}{\tau_o}\right)^2 + \left(\frac{\tau_\infty}{\tau_o}\right)^4\right]^{1/2} - 1\right\} \quad \ldots\ldots (47)$$

the formula being valid for τ_∞ less than 60 to 70 per cent of τ_o. Consequently, closure initiates at $\Delta\tau_\infty/\tau_\infty = 1.015$ for $\tau_\infty/\tau_o = 0.2$, at $\Delta\tau_\infty/\tau_\infty = 1.065$ for $\tau_\infty/\tau_o = 0.4$, and at $\Delta\tau_\infty/\tau_\infty = 1.105$ for $\tau_\infty/\tau_o = 0.6$. The closure ratio must increase rapidly as the remote stress approaches the limit load, as it is clear that its value would then approach two for the crack in an infinite solid. Once closure of a tensile crack initiates, relatively large compressive stresses would be expected necessary to cause much further reverse flow; thus, the above numerical results set approximate limits on the amount of load variation which should be considered responsible for cyclic plastic flow under tension-compression load cycles. A more exact analysis, based, say, on the discrete surface of tensile yielding model and following through the calculations after closure initiates at the crack midpoint, would be useful for the interpertation of fully reversed loading fatigue results.

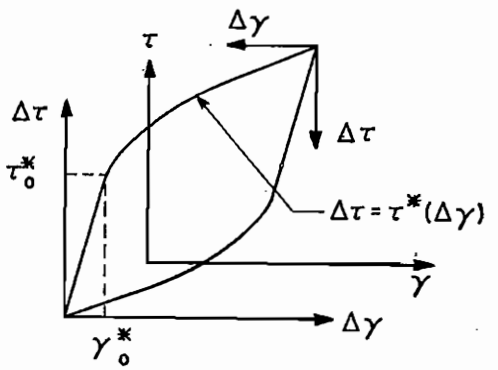

FIG. 23—*Stable hysteresis loop.*

The anti-plane shear work-hardening results for monotonic loading may similarly be extended to cyclic loadings, when stress-strain relations in the cyclic plasticity zone may be described as the traversal of stable hysteresis loops (Fig. 23) for which the stress and strain variations following a load reversal are related by a law independent of the maximum amplitudes of the loops. Morrow [*34*] has suggested such relations between stress and strain variations as good approximations to experimental results for cyclic plastic straining under zero mean load after a small per cent of the low cycle fatigue life is passed. Whether similar results hold in the presence of a mean stress is unclear. As in Fig. 23, τ_o^* and γ_o^* are the yield stress and strain in a coordinate system $\Delta\tau$, $\Delta\gamma$ measured from a point of load reversal; in the plastic range, $\Delta\gamma > \gamma_o^*$, $\Delta\tau = \tau^*(\Delta\gamma)$. The solution for stress and strain variations is identical in form to that for monotonic loading. Thus, employing a polar strain coordinate system $\Delta\gamma$, ϕ analogous to Fig. 10*c*, the small scale reverse yielding solution follows the form of Eqs 21; in the reverse plastic zone:

$$\left.\begin{aligned} x &= X^*(\Delta\gamma) + R^*(\Delta\gamma)\cos 2\phi \\ y &= R^*(\Delta\gamma)\sin 2\phi \end{aligned}\right\} \quad \ldots\ldots\ldots\ldots (48a)$$

where

$$\left.\begin{aligned} X^*(\Delta\gamma) &= \frac{(\Delta K_{III})^2}{2\pi(\tau_o^*)^2}\left\{2\gamma_o^*\tau_o^*\int_{\Delta\gamma}^{\infty}\frac{du}{u^2\tau^*(u)} - \frac{\gamma_o^*\tau_o^*}{\Delta\gamma\tau^*(\Delta\gamma)}\right\} \\ R^*(\Delta\gamma) &= \frac{(\Delta K)_{III}^{\ 2}}{2\pi(\tau_o^*)^2}\frac{\gamma_o^*\tau_o^*}{\Delta\gamma\tau^*(\Delta\gamma)} \end{aligned}\right\} \quad \ldots\ldots (48b)$$

The geometric interpretation of Fig. 11 applies for cyclic flow also. Lines of constant cyclic strain variation are circles of radius $R^*(\Delta\gamma)$ centered a distance $X^*(\Delta\gamma)$ ahead of the crack. The perfect plasticity cyclic solution of Eqs 44 is recovered by setting $\tau^*(\Delta\gamma) = \tau_o^* = 2\tau_o$. As an example, for a power law relating stress and strain variations in the hardening range,

$$\Delta\tau = \tau_o^*(\Delta\gamma/\gamma_o^*)^N \quad \ldots\ldots\ldots\ldots\ldots\ldots (49a)$$

the cyclic strain variation in the reverse flow plastic region ahead of the crack caused by a load fluctuation ΔK_{III} is

$$\Delta\gamma_{yz}(x,0) = \gamma_o^*\left[\frac{(\Delta K_{III})^2}{(1+N)\pi(\tau_o^*)^2 x}\right]^{1/(1+N)} \quad \ldots\ldots\ldots (49b)$$

The stress concentration of a crack has been assumed to remain infinite in discussing unloading and cyclic loading solutions. Actually the large strains generated result, as has been seen, in finite crack opening displacements so that a small range of elastic unloading may be expected. A rough estimate of this range may be had by assuming the crack to open into a narrow elliptical shape with a root radius of curvature given by the crack opening displacement corresponding to the maximum applied stress σ_∞. Then employing the stress concentration factor of Eq 8*a* for the ellipse of length $2a$ in a large body, the elastic unloading range $\Delta\sigma_\infty$ prior to reverse flow at the crack tip is given by

$$2\sigma_o = \Delta\sigma_\infty[1 + 2(a/u_o)^{1/2}] \approx 2\Delta\sigma_\infty(a/u_o)^{1/2} \quad \ldots\ldots\ldots (50a)$$

Estimating the opening displacement from the discrete surface of tensile yielding model, Eq 34*c*, the ratio of the elastic unloading range to the maximum applied stress is

$$\frac{\Delta\sigma_\infty}{\sigma_\infty} = \left\{\frac{(\kappa+1)\sigma_o}{2\pi G}\left(\frac{\sigma_o}{\sigma_\infty}\right)^2 \log\left[\sec\left(\frac{\pi\sigma_\infty}{2\sigma_o}\right)\right]\right\}^{1/2} \quad \ldots\ldots\ldots (50b)$$

At low stress levels this becomes independent of σ_∞/σ_o, and for plane stress conditions the elastic range is given by

$$\Delta\sigma_\infty = (\pi\epsilon_o/2)^{1/2}\sigma_\infty \approx 1.25\,\epsilon_o^{1/2}\sigma_\infty \quad \ldots\ldots\ldots\ldots (50c)$$

where $\epsilon_o = \sigma_o/E$ is the yield strain in tension. The result is not highly dependent on the maximum stress over a substantial range; at $\sigma_\infty/\sigma_o = 0.8$ the numerical factor is 1.49 and at $\sigma_\infty/\sigma_o = 0.95$ it is 1.89. There is a rather fast transition as fully developed plasticity is attained, for the numerical factor approaches infinity at the limit load for the perfectly plastic model. This would suggest that overall plastic straining is required to cause sufficient crack blunting for purely elastic response to all but the small load variations. Taking $\epsilon_o = 0.002$, as appropriate for a yield stress of 60 ksi in steel, below limit conditions the elastic range is roughly 5 per cent of the maximum applied stress. An approximately equal figure results for the elastic range following the application and complete removal of a maximum stress σ_∞.

A further approximate analysis of crack blunting may be based on the anti-plane shear perfect plasticity solution for a rounded end notch of root radius ρ. Recalling that stress free boundaries are now semicircular and taking $x = 0$ at the rounded notch tip, in the plastic region $0 < x < \omega - \rho$,

$$\gamma_{yz}(x,0) = \frac{\gamma_o \omega}{\rho + x} = \frac{u_o}{\rho + x} \quad \ldots\ldots\ldots\ldots\ldots (51a)$$

where u_o is the crack opening displacement for monotonic loading. Here ρ is considered of negligible size compared to the plastic zone size. Assuming for the moment that the radius of curvature is fixed, for a monotonic load increment resulting in du_o,

$$d\gamma_{yz}(x,0) = \frac{du_o}{\rho + x} \quad \ldots\ldots\ldots\ldots\ldots\ldots (51b)$$

It turns out that this expression is also correct for unloading and subsequent reloading if variations in u_o are computed according to Eq 44. Now if one assumes a similar relation to hold for tensile cracks, the root radius of curvature would appropriately be chosen as the current crack opening displacement resulting from the prior deformation history and computed according to equations based on the neglect of crack tip blunting, as displacements are an integrated effect. Thus,

$$d\epsilon_y(x,0) \approx \frac{d\rho}{\rho + x} \approx \frac{du_o}{u_o + x} \quad \ldots\ldots\ldots\ldots\ldots (52a)$$

At the notch tip this results in $d\epsilon_y = d\rho/\rho$, which would appear to be of approximately the correct form. Thus integrating under the assumption that $\rho = u_o = 0$ prior to any load application (the only other plausible assumption is an atomic spacing; any further crack blunting must be assumed the result of plastic deformation although many authors prefer ascribing a fixed nonatomic radius to cracks), after any loading sequence which results in a final opening displacement u_o

$$\epsilon_y(x,0) \approx \log\left(1 + \frac{u_o}{x}\right) \quad \ldots\ldots\ldots\ldots\ldots\ldots (52b)$$

Since u_o is on the order of a yield strain times a plastic zone dimension, the logarithm behaves as u_o/x at distances much greater than the yield strain times plastic zone size, in agreement with the shear result (Eq 51*a*). For a load variation which changes the opening displacement from $u_{o\,\min}$ to $u_{o\,\max}$, the corresponding strain variation is from Eq 52*a*

$$\Delta\epsilon_y(x,0) \approx \log\left(\frac{u_{o\,\max} + x}{u_{o\,\min} + x}\right) \quad \ldots\ldots\ldots\ldots\ldots\ldots (53a)$$

Now, regardless of the model employed, the crack opening displacement for small scale yielding takes the form

$$u_o = \alpha \frac{\epsilon_o K_I^2}{\sigma_o^2} \quad \ldots\ldots\ldots\ldots\ldots\ldots\ldots\ldots (53b)$$

for monotonic loading, where α is a numerical constant. Suppose that a peak stress intensity factor $K_{I\,\max}$ is applied and removed, and then further cyclic loads are applied over a range from zero to ΔK_I; then

$$u_{o\,\min} = \frac{\alpha}{2} \frac{\epsilon_o (K_{I\,\max})^2}{\sigma_o^2}; \qquad u_{o\,\max} = \frac{\alpha}{2} \frac{\epsilon_o (\Delta K_I)^2}{\sigma_o^2} + u_{o\,\min} \ldots (53c)$$

At the notch tip $x = 0$,

$$\Delta\epsilon_y(0,0) \approx \log\left[1 + \left(\frac{\Delta K_I}{K_{I\,\max}}\right)^2\right] \quad \ldots\ldots\ldots\ldots (53d)$$

Setting $\Delta\epsilon_y = 2\epsilon_o$ and taking the stress intensity factor proportional to a remotely applied stress, this equation closely approximates the estimate of the elastic unloading range given previously. When $K_{I\,\max} = \Delta K_I$ (no peak load), the strain variation at the notch tip is $\Delta\epsilon_y \approx 0.69$. While this result is independent of the load level, the size of the region ahead of the notch affected by high strains is not. This falls off to $\Delta\epsilon_y \approx 0.22$ when the peak load is twice the subsequent cyclic amplitude, and $\Delta\epsilon_y \approx 0.04$ when a peak load of five times the subsequent amplitude is applied. Smaller values develop if the peak is out of the small scale yielding range. While one hesitates to attempt quantitive comparisons due both to the highly approximate nature of the calculations and the lack of data on the strain amplitude necessary to continuously propagate a crack, this marked reduction in local cyclic strain by a peak loading does appear consistent with the experimental results of Donaldson and Anderson [*35*], who found that high peak loads could effectively stop crack propagation for a large number of subsequent load cycles.

General Features of Fatigue Crack Growth

The growth of fatigue cracks prior to catastrophic fracture is conveniently divided into processes of initiation as microcracks and propagation as macrocracks. The latter propagation stage is of primary interest here. Thompson and Wadsworth [*39*], Avery and Backofen [*11*], and Grosskreutz [*12*] have surveyed work on micromechanisms relating to crack initiation. Commonly, initiation occurs at a free surface. The cyclic component of tensile stress at a surface point sets up alternating shear stresses, maximum on 45-deg planes with the tensile direction. Conveniently oriented slip systems respond by the formation of slip bands resulting in a roughened surface topology in the form of intrusions and extrusions. These apparently act as stress concentrators so that cracking occurs along the slip bands. Interior initiation sites at grain boundaries may occur in the presence of overall cyclic plastic deformation. While no clear demarcation point exists, cracks initiated at 45 deg with the tensile direction tend to propagate as macrocracks on planes perpendicular to the tensile direction. Factors such as corrosive environments and fabrication imperfections in practical structures tend to limit the importance of initiation processes; cracks may frequently be present from the start [*35*].

Striation formation [*12,41*] is observed on portions of fatigue crack surfaces perpendicular to the tensile direction, both in metals and polymers [*42*]. Estimates of striation spacings agree well with macroscopic growth per cycle measurements [*41*], so that fatigue crack growth would appear continuous at least in regions of striation formation. This need not always be the case; Frost [*40*] reports continuous fatigue intermingled with occasional spurts of short fracture advances in some cases. Laird and Smith [*43*] have demonstrated a mechanism of striation formation through crack tip deformation under large cyclic stresses; the observed deformation pattern is much like what might be expected from the slip line field of Fig. 21. A fatigue crack mode transition from a 90 to 45-deg orientation of the crack surface with respect to the tensile direction is observed in sheet materials at sufficiently high load levels [*40,44*], similar to the plane stress fracture mode transition [*45*] under monotonic loadings. Hertzberg [*41*] found no striations on 45-deg portions of the fatigue crack surfaces; ductile "dimples" appear instead, elongated in a direction perpendicular to the direction of crack advance.

A survey of work on the relation of continuum considerations to models of microstructural "damage" accumulation and material separation is given in the next section. For the present we examine what general conclusions on fatigue crack growth follow the elastic-plastic analyses discussed earlier, without specific reference to microstructural considerations and fine details of cyclic stress and strain distributions. While

conclusions are more limited in detail, the groundwork is firmer. The varying results of Figs. 8 and 9 raise valid cause for doubt that continuum plasticity solutions can confidently be extrapolated to the fine scale of the microstructure. For example, a cyclic stress variation of one fifth the yield stress sets up a cyclic plasticity zone of roughly one hundredth of the crack depth in size; this figure is in the size range of one or a few grains for cracks less than an inch in depth.

One of the central results emerging from the analyses of all the elastic-plastic models is that, for small scale yielding, the plastic deformation is

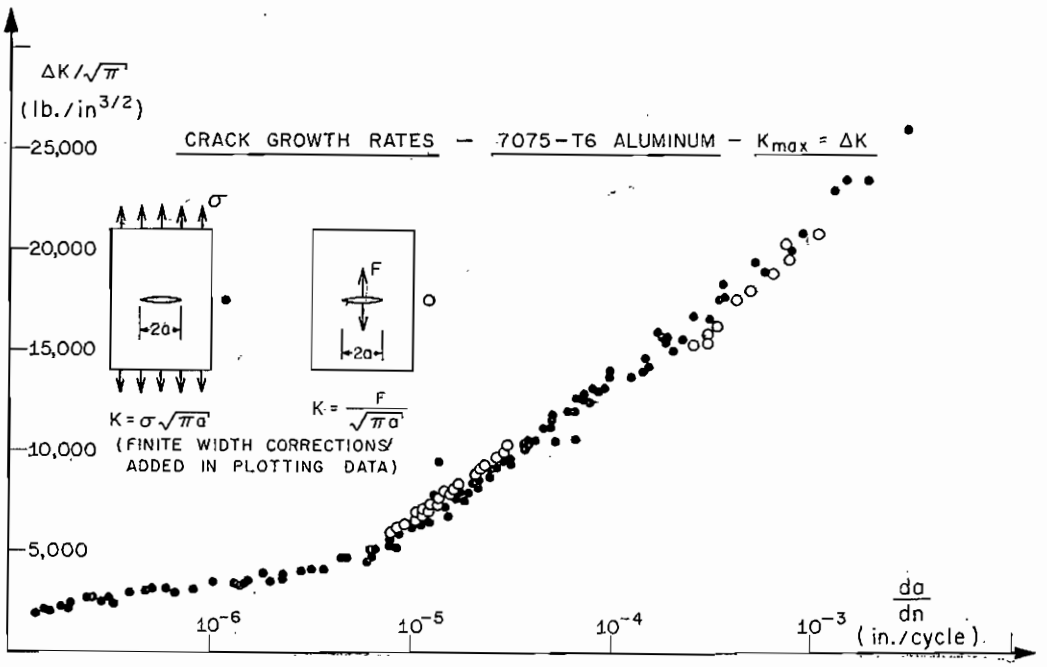

FIG. 24—*The correlation of crack growth rate in terms of stress intensity factor variation for 7075 T-6 aluminum (maximum load equal to load range) (Ref 47).*

entirely determined by the history of variation in the Irwin stress intensity factor. Thus two different cracked bodies with identical material properties (and sheet thickness where three dimensional considerations govern, as in plane stress yielding) will exhibit identical fatigue crack extensions if each is subjected to the same small scale yielding range time history of variation in elastic stress intensity factor. Paris, Gomez, and Anderson [*46*] first proposed a correlation of this type; a series of subsequent studies by Paris [*47*], Paris and Erdogan [*6*], Donaldson and Anderson [*35*], Schijve and Jacobs [*48*], and Schijve et al [*49*], employing both their own data and that of several other investigators, have amply documented the validity of this approach. McEvily and Illg [*50*] developed an equivalent approach based on the variation of the elastically predicted maximum concentrated stress, viewing a crack as a notch with

a fixed root radius sufficiently small so that the direct relation with stress intensity factors noted in Eq 8*c* applies. (Incidentally, most of the literature on fatigue crack growth employs a definition of the stress intensity factor which differs by a factor of $\pi^{1/2}$ from that given here.) A cyclic loading may be characterized by the maximum load value, $L_{\max}$, and the

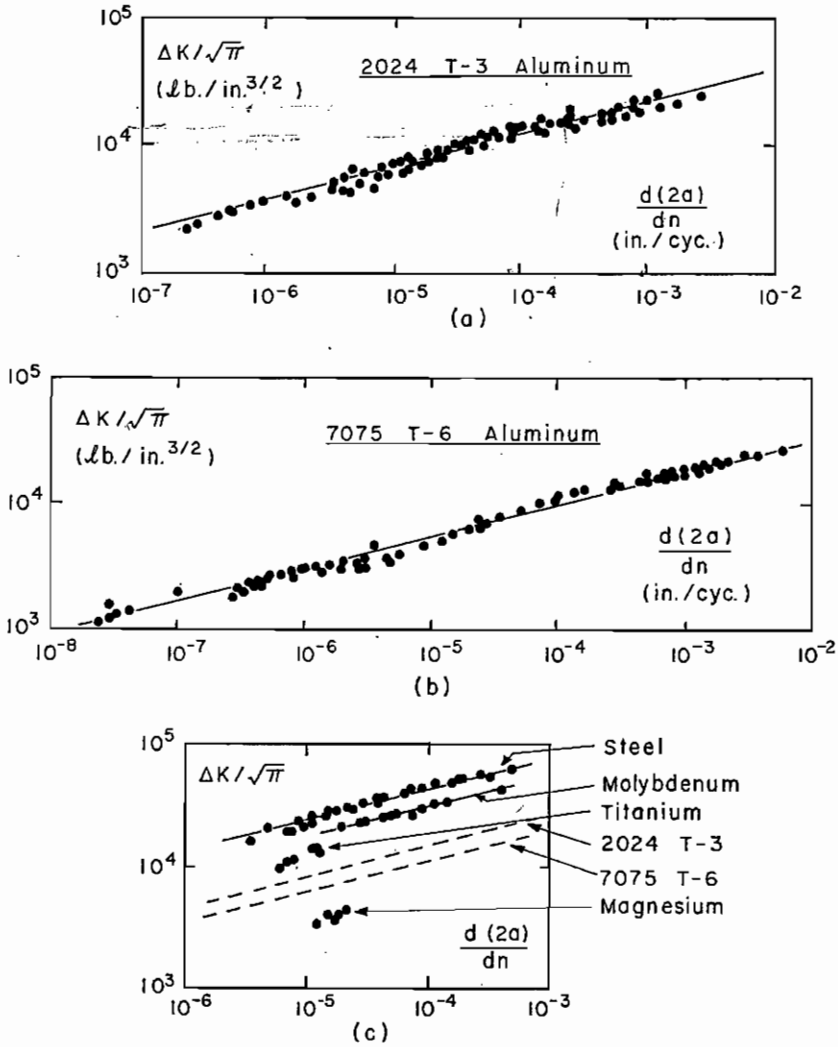

FIG. 25—*Crack growth rates in terms of stress intensity factor variation for several materials* (*Refs* 6 *and* 47).

load range, ΔL. When both the maximum plastic zone size and cyclic plastic zone size are in the small scale yielding range, the loadings and planar geometry of the cracked body are sensed at the crack tip only through the maximum, $K_{\max}$, and range, ΔK, in the stress intensity factor. The maximum value may be represented in the dimensionless form

$$\lambda = \frac{K_{\max}}{\Delta K} = \frac{L_{\max}}{\Delta L} \quad \ldots\ldots\ldots\ldots\ldots\ldots (54a)$$

the latter following since stress intensity factors, coming from linear boundary value problems, are directly proportional to applied loads times functions of the current geometry. Thus, where da/dn is the extension of a crack tip per cycle of loading,

$$\frac{da}{dn} = f(\Delta K,\lambda) \quad \ldots\ldots\ldots\ldots\ldots\ldots\ldots\ldots (54b)$$

for the comparisons of crack growth rates when all other material characteristics are held constant. One of the most striking verifications of a result of this form was provided by Paris [*47*] on the basis of data on 7075T-6 aluminum with $\lambda = 1$. Figure 24 (Fig. 1 of Ref *47*) shows crack growth rates as a function of stress intensity factor range for two central crack configurations, one [*35*] loaded by wedge forces F per unit sheet thickness and the other [*50*] by a tensile stress σ. Without corrections for finite width (included along lines of the infinite array analysis of Fig. 18 in plotting the data), the stress intensity factors are

$$K = \sigma(\pi a)^{1/2} \qquad \text{and} \qquad K = F(\pi a)^{-1/2} \ldots\ldots\ldots\ldots (55)$$

ΔK increases with crack length for a constant tensile stress variation and decreases with crack length for a constant wedge force variation. While the loadings are about as different as could be imagined, both cases fall on essentially the same curve.

Figures 25*a*, *b*, and *c*, from Refs *6* and *47*, demonstrate a similar success of the stress intensity factor variation in unifying crack growth rate data for several materials. Figure 25*a* represents the results of five independent investigations on 2024T-3 aluminum. Figure 25*b* replots in a similar fashion that of Fig. 24 on 7075T-6 aluminum, with the results of another investigation added. The two aluminum alloys plots are represented by straight lines in Fig. 25*c*, which shows additional data on magnesium, titanium, molybdenum, and steel. The scatter is largely due to a failure to distinguish, in these plots, effects due to maximum loads greater than the load variation range, differences in test frequency, differences in sheet thicknesses, and mode transition from 90 to 45 deg with the tensile axis. The plots being log-log, straight lines are indicative of power law relations. All of the straight lines drawn have a slope of four so that, as noted by Paris and Erdogan [*6*], the broad trend of the data is represented by a crack growth rate proportional to the fourth power of the stress intensity factor variation. At the same time, it is clear from the figures that a law of this type may provide a poor approximation over limited ranges of data which may be of interest in particular applications.

All perfect plasticity models discussed earlier predict a dependence of the cyclic plastic flow only on the variation in stress intensity factor; the same conclusion follows for work-hardening behavior when stable

hysteresis loops of the type described in connection with Fig. 23 are formed. Thus, it is not surprising that the maximum load achieved is a minor variable, as compared to the load range, in determining fatigue crack growth rates. An obvious exception is when the maximum is less than the range so that crack closure may intervene, as in the fully reversed loading tests by Illg and McEvily [*51*]. The small range of compressive loading prior to crack closure predicted by Eq 47 would suggest that for reversed loadings in and somewhat above the small scale yielding range, the load variation should be counted simply as the tensile part of the cycle; the interpretation appears justified as crack growth rates are only slightly faster for fully reversed loadings [*51*]. Aside from the possibility of crack closure, the effect of different maximum loads with the same load variation is to increase, with increasing maximum levels, the average strain distribution about which the cycling takes place. While perfect plasticity predicts a zero mean stress in the cyclic plastic zone, the effect of hardening for a hysteresis loop shift in the direction of the monotonic loading stress, as in Fig. 23, would be to place a biasing average stress distribution, more intense with increasing maximum level in the cyclic plastic zone.

Judging from the data of Schijve et al [*49*] on 2024T-3 under various ratios λ of maximum load to load range, at a given range of variation of the stress intensity factor the crack growth rate is tripled by doubling λ from 2 to 4. For comparison, a doubling of the stress intensity factor range of variation increased the crack growth rate by a factor between 10 and 15. Results at a fixed value of λ and sheet thickness, as by Schijve et al [*49*], greatly reduce the scatter in plots such as Fig. 25*a*. Paris [*52*] has tabulated values of the coefficient in a fourth power law description of crack growth rates for several materials and conditions. He finds an increase in the ratio of maximum to range from 1 to 4.5 increases growth rates, at the same stress intensity factor range, by a factor of roughly 10 in both 2024T-3 and 7076T-5. An increment by a factor of 4.5 in the stress intensity factor range increases growth rates by a factor of approximately 200 to 400. Frequency effects are slight in aluminum alloys, as might be expected from their relatively rate independent stress-strain behavior. An increase from 20 cpm to 20 cps roughly doubles [*52*] growth rates in 2024T-3.

Liu [*44*] has proposed that the fatigue crack mode transition from a 90 to 45-deg orientation with the tensile direction in sheet materials may be explained as a transition from plane strain (Figs. 20 and 21) to plane stress (Fig. 19) plasticity conditions, an extension of Irwin's [*45*] approach to fracture mode transition. Plane stress conditions may be expected to initiate when the plastic region becomes sufficiently large so that 45-deg shearing is kinematically possible. Equivalently, one then expects mode transition at a constant ratio of plastic zone dimension to sheet thick-

ness, t, as found by Liu [*44*] and Hertzberg [*41*] in cases where $K_{max} = \Delta K$, and the plastic zone dimension was estimated as proportional to the square of the ratio of stress intensity factor to yield stress. Results reported by Hertzberg would lead to a maximum plastic zone dimension equal to the sheet thickness and a reversed zone size of about one quarter the sheet thickness at transition, whether computed according to the discrete slip line model of Eq 38*a* (with the plastic zone size now counted as twice the slip line length) or the surface of tensile yielding model of Eq 31*a*. Broek and Schijve [*53*] found that a similar idea, for various cases of a maximum load greater than the load range, did not accurately predict the mode transition; the ratio of both maximum and cyclic zone sizes to thickness decreased with increasing thickness. They also report a

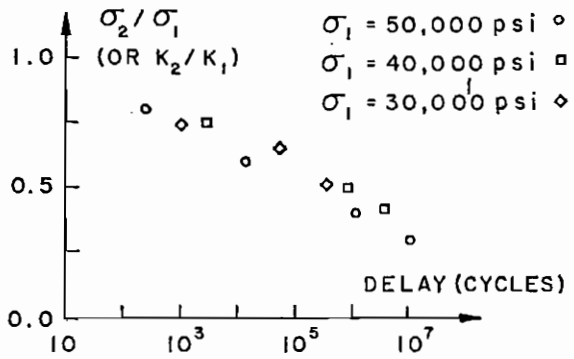

FIG. 26—*Delay affects in 7075 T-6 aluminum crack propagation due to reduction of stress range from σ_1 to σ_2 (data from Ref* 54).

systematic increase in growth rates with increasing sheet thicknesses prior to transition, although the effect becomes obscured after development of the inclined 45-deg fatigue crack surface.

The success in correlating crack growth behavior with stress intensity factor variation, as predicted by the mechanics analyses, may also be expected in situations of similar variations in stress intensity factors due to complicated deterministic or random loadings. Loadings with varying ranges introduce, however, an additional complication in that a sudden shift from a large to small range of load variation tends to stop crack extension from a few hundred to a few million load cycles [*35*,*54*]. Hardrath [*54*] has reported the results of tests on 7075T-6 aluminum in which a stress cycling range from zero to σ_1 is suddenly followed by a cycling range from zero to σ_2. As expected, for $\sigma_2 > \sigma_1$ the crack growth rate immediately adjusts to that corresponding to the latter stress range; delays result for $\sigma_2 < \sigma_1$. Hardrath's suggestion that the presence of residual compressive stresses near the crack tip is responsible for delays

appears to lack support from the plasticity analyses. For all the perfectly plastic models and for the stable hysteresis loops work-hardening model, the zone of cyclic plastic deformation as well as cyclic strain variations within this zone are unaffected by the prior load level, so that the residual stress argument would at most lead to an effect comparable to the slight consequences of changing the mean load level. A more plausible explanation would be based on the blunting of the crack tip by large deformations. When both σ_1 and σ_2 are in the small scale yielding range, the analysis in connection with Eq 53*d* suggests that the strain variations at the blunted crack tip depend only on the ratios of the stress intensity factors K_1 and K_2 or equivalently in this case on the ratio σ_1/σ_2, and not on the current crack length and separate ratios of σ_1 and σ_2 to the yield stress. Supposing the delay number of cycles to depend only on the reduced strain variation at the crack tip, a unique relation between delay time and stress ratio σ_1/σ_2 would be expected from the argument based on crack blunting. This conclusion appears roughly verified by the replot of Hardrath's data in Fig. 26. The largest prestress, σ_1, is 50,000 psi which is about 70 per cent of the yield stress so that Figs. 7 and 17 appear to justify the use of small scale yielding results as the calculation is based on crack opening displacements. Perhaps the systematically shorter delays at the same load ratio for the highest prestress is due to a higher average strain, about which variations take place, at the blunted crack tip.

For random loadings in the small scale yielding range, crack extensions may be expected identical in separate configurations if each crack tip experiences statistically identical variations in stress intensity factor. Paris [*47*] has displayed data verifying such a postulate for narrow bandwidth random loadings of geometrically similar power spectra, but different root mean square (rms) stress levels varying from 0.03 to 0.05 of the yield stress. The scatter is slightly larger than for cyclic loadings, possibly due to the enhanced likelihood of severe tip blunting at the higher rms levels. Although no computations of the statistical distribution of plastic strain variations have appeared (these could easily be provided for the various perfectly plastic models through a relatively simple computer program coupled with digitally generated random loadings), it appears reasonable on the basis of unloading and cyclic loading solutions to assume that the plastic deformations are controlled primarily by the distribution of rises and falls [*55,56*], ΔK, in the stress intensity factor. Rice et al [*47,56*] and Smith [*57*] have shown that crack growth rates may be correlated in terms of averages in stress intensity factor rise and fall heights, ΔK, for both narrow bandwidth random loadings and for doubly peaked (two dominant frequencies) wide bandwidth loadings. When correlated in this way all the random load crack growth rate data appear to fall on roughly the same curve, in spite of the great differences in waveform appearance for the different random loadings. But neither

random load crack growth rates, nor their general trend of variation with averages of ΔK, agree with cyclic loadings crack growth rates correlated in the same way. This suggests that it is not so much the waveform appearance, but rather the very introduction of randomness in load sequencing, which creates differences in comparison to the cyclic loading case. Hardrath [*54*] and Hardrath and Naumann [*58*] have indicated the differences in fatigue life resulting from similar load amplitude distributions programmed in different nonrandom sequences.

Erdogan and Roberts [*59*] reported a study of crack growth in thin plates subjected to fully reversed bending loads, and obtained a similar correlation of propagation rates in terms of the variation of a stress intensity factor defined through elastic solutions for plate bending. Their comparison with the tensile case suggested that for a given remotely applied stress range on the surfaces of a plate under bending, the propagation rate is approximately that which would result from one half that stress range applied in direct tension to a geometrically similar cracked plate. For identical stress ranges, propagation rates under direct tension are about 10 to 16 times faster than those for bending. Erdogan and Roberts also gave an approximate analysis of plastic yielding, based on an idea similar to the discrete surface of tensile yielding model, which suggested that the cyclic plastic zone for a given surface stress range in bending is equal in size to the zone resulting from one half that stress range applied in direct tension.

No single parameter plays the role of the elastic stress intensity factor, in determining the crack tip plasticity, when yielding is on a large scale compared to planar geometric dimensions. Thus crack growth rates may be predicted or estimated from data collected in the small scale yielding range only in conjunction with a reliable theory of crack propagation. Some progress may still, however, be anticipated from continuum considerations alone. The small scale yielding range for load cycling is double that for monotonic load application. Thus to the extent that the maximum applied load is a secondary variable in comparison with load range, situations may be expected in which the stress intensity factor variation correlates growth rates even though the total plastic region is outside the small scale yielding range. Further, although adequate experimental data to check such hypotheses are not available, one might expect that in the large scale yielding range crack growth rates may be correlated by such parameters as the maximum and cyclic plastic zone sizes or crack opening displacements, both of which are equivalent to the maximum stress intensity factor and its variation at low load levels. Some orderings of deviations from small scale yielding range growth results are also predictable. From Figs. 6 and 7, along with their interpretations for cyclic loadings, the small scale yielding solution always underestimates actual results for remotely applied stress loadings, the underestimate being

more severe with the smaller crack length to width ratios. Thus growth rates from small scale yielding tests conducted with long cracks and low net section stresses tend to underestimate rates at the same stress intensity factor when large scale yielding occurs, and for configurations with the same (high) net section stress and stress intensity factor, cracks grow faster for the smaller crack length to width ratios. A large scale yielding solution for wedge loadings as in Fig. 24 may be obtained through known general methods [7] for the discrete surface of tensile yielding model. It turns out in this case that the small scale yielding solution overestimates actual results, so that with wedge force loading growth rates are slower, with large scale yielding, than those occurring in a small scale yielding range test at the same stress intensity factor. Large scale yielding analyses are not available for situations involving net section yielding. This is an inherent difficulty with perfect plasticity models as unrestricted flow ensues; for work hardening an apparently tractable formulation [9] of the net section yielding problem is available in the anti-plane shear case, although mathematical difficulties have to date limited solutions to the case discussed in Part I. Consequently crack propagation under repeated overall plastic straining, as in low-cycle fatigue, currently is beyond the reach of reliable analytical treatments.

Theories of Fatigue Crack Growth

Obvious importance attaches to the prediction of crack growth rates in terms of continuum and microstructural variables for arbitrary load sequences. Only the studies of Head [60,61], McClintock [62], Rice [7,63], and Weertman [64] have attempted the direct use of elastic-plastic analyses, and none of these incorporated the possibility of crack blunting and delays which are known to occur with block loadings or peak overloads and probably form an integral part of fatigue crack growth under more general deterministic or random loading sequences. Thus, the work surveyed here is limited to nonvariable amplitude cyclic loadings and should be viewed as at most a start toward the problem of relating continuum analyses to material separation by fatigue.

Dimensional considerations were introduced by Frost and Dugdale [65] and Liu [66,67]. The relevant variables for a crack of length a in a large body are (assuming the maximum stress to equal the stress range)

$$\Delta\sigma,\ a,\ \sigma_o\ ,\ \epsilon_o\ ,\ \epsilon_f\ ,\ N,\ \frac{da}{dn}$$

where the elastic modulus is included implicitly through the yield strain ϵ_o, N is the hardening exponent or some other dimensionless variable (or set of variables) characterizing the hardening behavior, and ϵ_f is some characteristic fracture strain. Attention is limited to plane strain situations so that sheet thickness does not enter. With the assumption that

continuum variables *alone* control the extension per cycle at a crack tip, there results [*65–67*]

$$\frac{da}{dn} = af_1(\Delta\sigma/\sigma_o, \epsilon_o, \epsilon_f, N) \quad \ldots\ldots\ldots\ldots\ldots\ldots (56a)$$

where f_1 is a dimensionless function of its arguments. Liu [*67*] recognized the requirement of applied stress and current crack length entering only in the form of the stress intensity factor variation, $\Delta K = \Delta\sigma(\pi a)^{1/2}$, and therefore proposed

$$\frac{da}{dn} \propto a(\Delta\sigma)^2 \propto (\Delta K)^2 \quad \ldots\ldots\ldots\ldots\ldots\ldots (56b)$$

On the basis of a somewhat arbitrary modification of a result of Head discussed subsequently and the requirement of fitting samples of data with a growth rate proportional to crack length, Frost and Dugdale proposed

$$\frac{da}{dn} \propto a(\Delta\sigma)^3 \quad \ldots\ldots\ldots\ldots\ldots\ldots\ldots\ldots (56c)$$

a result contrary to predictions of continuum analyses in the small scale yielding range typical of high-cycle fatigue, but possibly indicative of the direction of the large yielding modifications necessary for stress ranges above about 80 per cent of the net yield stress. Paris and Erdogan [*6*] and Schijve and Jacobs [*48*] have amply documented the failure of these laws to fit the broad trend of crack growth rate data. For example, in Fig. 24 an increase in ΔK by a factor of 10, from 4400 to 44,000 lb·in.$^{-3/2}$, increases the growth per cycle by a factor very nearly equal to 10^4, from 3×10^{-7} to 2.5×10^{-3} in. Liu's result would predict an increase in growth per cycle by a factor of only 10^2, and the Frost and Dugdale result would increase growth by a factor between 10^2 and 10^3. Both fail by one or two orders of magnitude, although both can admirably fit limited portions of the available data [*6*]. Liu [*44,68*] has suggested that part of the difficulty may lie in the failure to distinguish between the plane stress and plane strain modes of crack growth in the general trend of the data, thus introducing sheet thickness as another length. The maximum stress intensity factor value cited above leads to a maximum plastic zone size of $\omega \approx 0.16$ in. in 7075T-6 aluminum, according to the discrete surface of tensile yielding model, Eq 31*a*. As noted earlier, this would correspond to mode transition in all sheets thinner than about 0.16 in.; however, the general fourth power trend of the data extends to lower load levels and at half the maximum stress intensity factor value the transition thickness would already be reduced to about 0.04 in. While Liu does give evidence [*44*] of different growth rates before and after transition, he does not verify (Eq 56*b*).

Equation 56*b* is the logical consequence, for the usual small scale yield-

ing situations, of an assumption that only continuum variables govern fatigue crack propagation. Its failure may be taken as a definite indication that another characteristic length, related to material separation, must enter a theory of crack growth. Calling l this characteristic length, a dimensional analysis incorporating the small scale yielding result that loads and geometry enter only through the stress intensity factor leads to

$$\frac{da}{dn} = \frac{(\Delta K)^2}{\sigma_o^2} f_2[(\Delta K)^2/(l\sigma_o^2), \epsilon_o, \epsilon_f, N] \quad (57)$$

f_2 being dimensionless. If several characteristic lengths enter, their ratios are understood included. When sheet thickness, t, enters as in the plane stress mode, an additional dimensionless parameter $(\Delta K)^2/(t\sigma_o^2)$ is included. For maximum loads different from the load range, the dimensionless ratio $\lambda = K_{\max}/\Delta K$ enters. As growth rates generally vary faster than $(\Delta K)^2$, any increase in l while holding other parameters constant serves to lower crack growth rates. The choice of l is related to the choice of a separation mechanism. McClintock [*62*] (see further), for example, takes l as the characteristic cell size formed by cyclic straining [*12*] and achieves a remarkable unity in predicting growth rates by taking this as the smallest size at which the concept of a homogeneous fracture strain retains meaning. Other choices lead to physically reasonable results. As material separation involves bond breakage and, in fatigue, possibly partial rehealing, l may be related to the surface energy or work per unit area in separating bonds (surface energy divided by a yield stress or elastic modulus has length dimensions). Thus picturing environmental effects as reducing surface energy through the formation of weak easily broken bonds with the environmental agent, similar to proposals by Westwood [*69*], known influences [*70,71*] of environments in reducing fatigue life would be expected. Hertzberg [*41*] reports no distinct surface markings indicative of a characteristic length in regions of striation formation, so that surface energy may indeed provide the appropriate length. Ductile dimples do occur, however, on fully developed plane stress fatigue surfaces and these might be the result of progressive void growth and coalescence under repetitive straining, similar to an observed mechanism of ductile rupture [*72*]. In this case the mean void nucleation site spacing would provide the characteristic length.

Head's [*60,61*] work on fatigue was done before treatments of plasticity near cracks were available and is based on drastic simplifying assumptions. A cracked body is viewed as a composite array of three types of continua. Taking infinitesimal elements of each of these types, material directly ahead of the crack is viewed as an array of independent rigid-plastic tensile bars, each hardening linearly from a yield stress σ_o to an ultimate stress σ_f at a modulus E_w. The material above and below the

crack and rigid-plastic bar array is viewed as an array of independent elastic tensile bars each carrying the remotely applied stress σ. The remotely applied stress is transmitted to the rigid-plastic bars both directly and through an array of elements transmitting load by shear. Head chose properties of the shear elements and lengths of the elastic tensile bars so that an elastic solution of the model properly gave the opening displacement at the center of the crack. The only shear elements activated are those above and below the crack and plastic zone, so that the stress on the line ahead of the crack turns out to equal the remotely applied stress outside the plastic region.

An approximate solution was then given for the crack growth rate due to a stress range $-\sigma$ to $+\sigma$, under the assumption that separation occurred when the rigid plastic elements cyclically hardened in the absence of a Bauschinger effect up to the ultimate stress σ_f. At low stress levels, $\sigma \ll \sigma_o$,

$$\frac{da}{dn} = \frac{E_w \sigma^3 a^{3/2}}{3E(\sigma_f - \sigma_o)(\sigma_o - \sigma)^2 l^{1/2}}, \qquad (\sigma \ll \sigma_o) \ldots\ldots (58a)$$

where $2l$ is the height of the rigid plastic elements in front of the crack. Head does not suggest how the constant l should be chosen. Contrary to the impression created by several summaries [*40,6*] of Head's work, the plastic zone size is not constant but rather given by

$$\omega = \frac{(la)^{1/2}}{2} \frac{\sigma}{\sigma_o - \sigma} \ldots\ldots\ldots\ldots\ldots\ldots (58b)$$

As the computation is for low stress levels it is appropriate to replace $\sigma_o - \sigma$ by σ_o so that Eq 58*a* gives a growth rate varying as the third power of the stress intensity factor and Eq 58*b* gives a plastic zone size proportional to the first power. The deviation in the latter result from dependence on the square of the stress intensity factor is clearly due to the artificial introduction of the length l. Frost and Dugdale obtained Eq 56*c* by assuming l proportional to crack length, but as Paris and Erdogan have noted [*6*] l must be chosen proportional to stress squared times crack length if it is to be interpreted as a plastic zone dimension. Head also provided a solution for the remotely applied stress in excess of the yield stress, $\sigma \geqq \sigma_o$:

$$\frac{da}{dn} = \frac{2E_w \sigma^3 a^{3/2}}{E\sigma_f(\sigma_f^2 - \sigma^2) l^{1/2}} \ldots\ldots\ldots\ldots\ldots\ldots (58c)$$

Aside from the drastic idealization of a continuum and the unidentified length, Head's proposed mechanism of separation by continuous work hardening up to a fracture stress may be questioned, as materials do not harden indefinitely under cycling straining [*12,34*] but rather tend to stabilize and in some cases to cyclically soften.

Rice [7,63] and Weertman [64] considered essentially identical models for fatigue crack growth, both based on the plasticity model of a discrete surface of tensile yielding or slip ahead of the crack. Tracing the deformation history of a particular point from when that point is first encompassed by the plastic zone to when the crack tip advances to that point, separation is assumed to occur when the total absorbed hysteresis energy equals a postulated critical value U^* per newly created surface area. Letting $\Delta u_y(x,0)$ be the plastic displacements of the discrete surface of tensile yielding per load reversal when the crack tip is at $x = 0$ and assuming the growth rate sensibly constant in a traversal of a zone ω^* of reversed deformation, the growth rate is given by

$$\frac{da}{dn} = \frac{4\sigma_o}{U^*} \int_0^{\omega^*} \Delta u_y(x,0)dx \quad \ldots\ldots\ldots\ldots\ldots (59a)$$

Restricting attention to the small scale yielding range and obtaining $\Delta u_y(x,0)$ by doubling the yield stress and strain in the monotonic loading solution, there results

$$\frac{da}{dn} = \frac{5\pi(\kappa+1)\sigma_o^2}{48U^*G}\left(\frac{\Delta K}{2\sigma_o}\right)^4 = \frac{5\pi(1-\nu^2)\epsilon_o\sigma_o}{96U^*}\left(\frac{\Delta K}{\sigma_o}\right)^4$$

$$= \frac{5\pi^3(1-\nu^2)\epsilon_o\sigma_o}{96U^*}\left(\frac{\Delta\sigma_\infty}{\sigma_o}\right)^4 a^2 \ldots (59b)$$

the latter forms using the plane strain value of $\kappa = 3 - 4\nu$. While the fourth power dependence resulting is in accord with the general trend of experimental results, the model does not provide a direct interpretation of the hysteresis energy U^* required per unit of newly created fatigue crack surface area. Choosing a best fit fourth power law to the data of Fig. 25*a*, $U^* \approx 6.3 \times 10^4$ lb·in./in.^{2} for 2024T-3 aluminum. For comparison, the energy absorbed in fracture of this material under monotonic loading is typically over two orders of magnitude smaller at about 3×10^2 lb·in./in.^{2} It is of interest to note that a difference in total ductility of the same order of magnitude (typically 100 to 1000 times) occurs in fully plastic push pull fatigue tests as opposed to monotonic fracture tests [73,62]. Perhaps the most serious objection here is the simplicity of the discrete surface of tensile yielding model; while the model no doubt gives accurate estimates of gross features of the plastic deformation such as zone size, crack opening displacement, and total hysteresis energy losses, all fine details of the plastic strain distribution are lost. Also, at high stress levels plastic regions tend to change shape so that the per cent of the hysteresis energy absorbed in regions very near the fracture surface will not be constant. Nevertheless, Wells [74] does find that a similar failure criterion based on energy absorbed at the crack tip (that is, yield stress times crack opening displacement) tends to correctly extend the

small scale yielding monotonic fracture criterion into the large scale yielding range.

McClintock [*62,14*] has developed a mechanics of crack extension by fatigue, stable slow growth, and catastrophic propagation, employing the anti-plane shear perfect plasticity solution and a failure criterion based on plastic strain accumulation over a "structural size" of the material. While valid objections might be raised to the relevance of these results for tensile loadings, we have seen that gross features of the plasticity are relatively insensitive to the deformation mode, and, indeed, his studies have provided the most satisfactory conceptual and quantitative basis for the entire range of observed tensile crack extension behavior in ductile materials. One of the less obvious results arising is the differentiation between strain increments due to crack extension under fixed loads as opposed to load variations at a fixed crack length. For example, in the case of an edge crack of length a in a large body remotely anti-plane sheared, the strain variation per unit crack length increment at fixed loads in the plastic region ahead of the crack tip is [*62*] (approximately)

$$\frac{\partial \gamma_{yz}(x,0)}{\partial a} = \frac{\gamma_o}{x}\left(1 + \frac{\omega}{a} + \log\frac{\omega}{x}\right) \quad \ldots\ldots\ldots\ldots (60)$$

where the crack tip is at $x = 0$ and ω is the plastic zone size accompanying monotonic load application. While the shear case probably tends to somewhat overestimate growth effects in tension, their inclusion results in a prediction of observed stable crack extensions prior to catastrophic fracture, more pronounced for increasing fracture ductility. Even at relatively low stress levels the stress intensity factor fails to uniquely characterize the plasticity when significant growth under fixed loads occurs; as a consequence the small scale yielding range for fractures controlled by the stress intensity factor is greatly reduced in very ductile materials under plane stress conditions where slow growth is most pronounced. Similar effects do not occur in fatigue crack propagation as strain variations due to load cycling at sensibly fixed crack lengths overwhelm the then negligible contributions due to growth. Growth effects would, however, be important in the few load cycles prior to catastrophic propagation in which the extension per cycle is comparable to the plastic zone size, but these comprise a negligible portion of the fatigue life.

The strain singularity at the crack tip forces one to work with a specially defined average strain over a finite region or to limit the region over which strain variations are considered consequential in determining separation. McClintock has chosen an average strain defined over a narrow wedge shaped region of angle $\delta\theta$ and length equal to the structural size, l:

$$\bar{\gamma}_{yz}(x,0) = \frac{1}{l^2\delta\theta/2}\int_0^l \gamma_{yz}(x + r,0) r\delta\theta dr \quad \ldots\ldots\ldots (61a)$$

Dropping the negligible crack growth contribution and assuming the growth rate sensibly constant in traversing the reverse yielding plastic zone, an adaption of the Coffin [75] criterion to varying amplitude plastic straining leads to the growth rate

$$\frac{da}{dn} = \int_0^{\omega^*} \left[\frac{\Delta\bar{\gamma}^p_{yz}(x,0)}{\gamma_f}\right]^2 dx \qquad (61b)$$

where $\Delta\bar{\gamma}^p_{yz}(x,0)$ is the variation in the plastic portion of the average plastic strain caused by a load variation, ω^* is the reversed plastic zone size, and γ_f is the monotonic fracture strain appropriate for the structural region of size l. There results [62] when $\omega^* \gg l$

$$\frac{da}{dn} = 7.5\left(\frac{\gamma_o}{\gamma_f}\right)^2 \frac{(\omega^*)^2}{l} \qquad (61c)$$

or for small scale yielding when the stress intensity factor variation, ΔK, controls the size of the reversed plastic zone,

$$\frac{da}{dn} = \frac{7.5}{16\pi^2}\left(\frac{\gamma_o}{\gamma_f}\right)^2 \frac{(\Delta K)^4}{l\tau_0^4} = \frac{7.5}{16}\left(\frac{\gamma_o}{\gamma_f}\right)^2 \left(\frac{\Delta\tau_\infty}{\tau_o}\right)^4 \frac{a^2}{l} \qquad (61d)$$

the latter form for the edge crack of length a or central crack of length $2a$ in a large body.

The result is not insensitive to the way the singularity is dealt with. For example, if only strain variations up to the point at which the distance to the crack tip is the structural size are considered of consequence in determining separation, which would be consistent with the treatment of monotonic fracture given by McClintock and Irwin [14], there results

$$\frac{da}{dn} = \int_l^{\omega^*} \left[\frac{\Delta\gamma^p_{yz}(x,0)}{\gamma_f}\right]^2 dx \qquad (62a)$$

And integrating with $\Delta\gamma^p_{yz} = 2\gamma_o(\omega^*/x - 1)$,

$$\frac{da}{dn} = 4\left(\frac{\gamma_o}{\gamma_f}\right)^2 \left[\frac{(\omega^*)^2}{l} - 2\omega^* \log\frac{\omega^*}{l} - l\right] \qquad (62b)$$

which resembles a fourth power dependence only for $\omega^* \gg l$. Converting the failure criterion into one of a critical hysteresis energy absorption, $\tau_o\gamma_f{}^*$ per unit volume,

$$\frac{da}{dn} = \frac{2}{\gamma_f{}^*}\int_l^{\omega^*} \Delta\gamma^p_{yz}(x,0)\, dx \qquad (62c)$$

and

$$\frac{da}{dn} = 4\frac{\gamma_o}{\gamma_f{}^*}\left[\omega^* \log\frac{\omega^*}{l} - (\omega^* - l)\right] \qquad (62d)$$

The variety of possibilities is clearly endless, further pointing to the re-

quirement of a better knowledge of the micromechanisms involved in material separation. Some results tabulated by McClintock tend to suggest the reasonableness of such estimates. Taking l equal to 5 μ (2×10^{-4} in.), a typical cell or subgrain size, the required ratio of the fracture strain to yield strain may be computed so as to fit experimental results to Eq 61*d*, replacing shear stresses by analogous tensile stresses. Within factors of about 2 to 4, known monotonic fracture strains for two aluminum alloys, two high strength steels, and mild steel appear accurately estimated, and the materials appear to be correctly ordered as to ductility [*62*].

The fact that Eqs 59 and 61 do not lead to major discrepancies lends hope that further progress may be made in relating continuum solutions to microstructural separation. Specifically, better continuum plasticity analyses and clearer pictures of separation mechanisms are needed. Crack blunting must be better modelled if varying amplitude loadings are to be handled. Probably the mathematical simplifications inherent in the boundary layer approach will make small scale yielding solutions the first obtained. As has been noted, these are adequate for virtually all of the usual high-cycle fatigue life. But the effects of large overloads and low-cycle fatigue loadings causing nonlocalized plastic flow cannot be handled until complete large scale yielding analyses are available.

Acknowledgment

The financial support of work leading to this report by a National Science Foundation Research Initiation Grant (GK-286) is gratefully acknowledged.

References

[*1*] H. Neuber, *Kerbspannungslehre* (English translation available from Edwards Bros., Ann Arbor, Mich.), 1st edition, Berlin, 1937, and 2nd edition, Berlin, 1958.

[*2*] G. N. Savin, *Stress Concentration Around Holes,* Pergamon Press, New York, 1961.

[*3*] G. R. Irwin, "Fracture Mechanics," *Structural Mechanics* (Proceedings of 1st Naval Symposium), Pergamon Press, New York, 1960.

[*4*] P. C. Paris and G. C. Sih, "Stress Analysis of Cracks," *Fracture Toughness Testing and Its Applications, ASTM STP 381,* Am. Soc. Testing Mats., 1965.

[*5*] N. I. Muskhelishvili, *Some Basic Problems of the Mathematical Theory of Elasticity,* P. Noordhoff, 1953.

[*6*] P. C. Paris and F. Erdogan, "A Critical Analysis of Crack Propagation Laws," *Transactions,* Am. Soc. Mechanical Engrs., Series D (*Journal Basic Engineering*), Vol 85, No. 4, 1963.

[*7*] J. R. Rice, "Plastic Yielding at a Crack Tip," *Proceedings,* International Conference Fracture, Sendai, Japan, 1965.

[*8*] J. R. Rice, "Contained Plastic Deformation Near Cracks and Notches Under Longitudinal Shear," *International Journal of Fracture Mechanics,* June, 1966.

[*9*] J. R. Rice, "Stresses Due to a Sharp Notch in a Work Hardening Elastic

Plastic Material Loaded by Longitudinal Shear," *Journal of Applied Mechanics.* (to appear, *ASME Paper 67-APM-1*).

[*10*] J. R. Rice, "On the Theory of Perfectly Plastic Anti-Plane Straining," *Technical Report NSF GK-286/2,* Brown University, March, 1966.

[*11*] D. H. Avery and W. A. Backofen, "Nucleation and Growth of Fatigue Cracks," *Fracture of Solids,* John Wiley & Sons, Inc., New York, 1963.

[*12*] J. C. Grosskreutz, "A Critical Review of Micromechanisms in Fatigue," *Fatigue—An Interdisciplinary Approach,* Syracuse University Press, Syracuse, N.Y., 1964.

[*13*] W. Prager and P. G. Hodge, Jr., *Theory of Perfectly Plastic Solids,* John Wiley & Sons, Inc., New York, 1951.

[*14*] F. A. McClintock and G. R. Irwin, "Plasticity Aspects of Fracture Mechanics," *Fracture Toughness Testing and Its Applications, ASTM STP 381,* Am. Soc. Testing Mats., 1965.

[*15*] J. A. Hult and F. A. McClintock, "Elastic-Plastic Stress and Strain Distribution Around Sharp Notches Under Repeated Shear," 9th International Congress Applied Mechanics, Vol 8, Brussels, 1956.

[*16*] G. R. Irwin and M. F. Koskinen, discussion and author's closure to Ref *17.*

[*17*] M. F. Koskinen, "Elastic-Plastic Deformation of a Single Grooved Flat Plate Under Longitudinal Shear," *Transactions,* Am. Soc. Mechanical Engrs., Series D (*Journal Basic Engineer*), Vol 85, 1963.

[*18*] H. Neuber, "Theory of Stress Concentration for Shear Strained Prismatical Bodies with Arbitrary Non-Linear Stress Strain Law," *Journal Applied Mechanics,* Vol 28, December, 1961.

[*19*] J. C. Grosskreutz, "A Theory of Stage II Fatigue Crack Propagation," *Report AFML-TR-64-415,* Air Force Materials Laboratory, March, 1965.

[*20*] V. Weiss, "Analysis of Crack Propagation in Strain-Cycling Fatigue," in *Fatigue—An Interdisciplinary Approach,* Syracuse University Press, Syracuse, N. Y., 1964.

[*21*] S. Rhee and F. A. McClintock, "On the Effects of Strain-Hardening on Strain Concentrations," *Proceedings,* 4th National Congress Applied Mechanics, Am. Soc. Mechanical Engrs., 1962.

[*22*] G. I. Barenblatt, "Mathematical Theory of Equilibrium Cracks in Brittle Fracture," in *Advances in Applied Mechanics,* Vol VII, Academic Press, New York, 1962.

[*23*] D. S. Dugdale, "Yielding of Steel Sheets Containing Slits," *Journal of Mechanics and Physics of Solids,* Vol 8, 1960.

[*24*] B. A. Bilby, A. H. Cottrell, and K. H. Swinden, "The Spread of Plastic Yield From a Notch," *Proceedings,* Royal Society A, Vol 272, 1963.

[*25*] J. N. Goodier and F. A. Field, "Plastic Energy Dissipation in Crack Propagation," *Fracture of Solids,* John Wiley & Sons, Inc., New York, 1963.

[*26*] F. A. Field, "Yielding in a Cracked Plate Under Longitudinal Shear," *Journal Applied Mechanics,* Vol 30, 1963.

[*27*] E. Smith, "Fracture at Stress Concentrations," *Proceedings,* International Conference Fracture, Sendai, Japan, 1965.

[*28*] L. M. Keer and T. Mura, "Stationary Crack and Continuous Distributions of Dislocations," *Proceedings,* International Conference Fracture, Sendai, Japan, 1965.

[*29*] G. T. Hahn and A. R. Rosenfield, "Local Yielding and Extension of a Crack Under Plane Stress," *Acta Metallurgica,* Vol 13, no. 3, 1965.

[*30*] B. A. Bilby and K. H. Swinden, "Representation of Plasticity at Notches by Linear Dislocation Arrays," *Proceedings,* Royal Society A, Vol 285, 1965.

[*31*] R. Hill, *The Mathematical Theory of Plasticity,* Clarendon Press, Oxford, 1950.

[*32*] D. C. Drucker, "A Continuum Approach to the Fracture of Metals," in *Fracture of Solids,* John Wiley & Sons, Inc., New York, 1963.

[*33*] F. A. McClintock, "Effect of Root Radius, Stress, Crack Growth, and Rate on Fracture Instability," *Proceedings,* Royal Society A, Vol 285, 1965.

[34] J. D. Morrow, "Cyclic Plastic Strain Energy and Fatigue of Metals," *Internal Friction, Damping, and Cyclic Plasticity, ASTM STP 378,* Am. Soc. Testing Mats., 1965.

[35] D. R. Donaldson and W. E. Anderson, "Crack Propagation Behavior of Some Airframe Materials," *Proceedings,* Crack Propagation Symposium, Cranfield, College of Aeronautics, 1962.

[36] J. L. Swedlow, M. L. Williams, and W. H. Yang, "Elasto-Plastic Stresses and Strains in Cracked Plates," *Proceedings,* International Conference Fracture, Sendai, Japan, 1965.

[37] R. Rosenfield, P. K. Dai, and G. T. Hahn, "Crack Extension and Propagation Under Plane Stress," *Proceedings,* International Conference Fracture, Sendai, Japan, 1965.

[38] D. R. Dixon and J. S. Strannigan, "Strain Distributions Around Cracks in Ductile Sheets During Loading and Unloading," *Journal Mechanical Engineering Science,* Vol 7, No. 3, 1965.

[39] N. Thompson and N. J. Wadsworth, "Metal Fatigue," *Advances in Physics* (Supplement to *Philosophical Magazine*), Vol 7, 1958.

[40] N. E. Frost, "The Growth of Fatigue Cracks," *Proceedings,* International Conference Fracture, Sendai, Japan, 1965.

[41] R. W. Hertzberg, "Application of Electron Fractography and Fracture Mechanics to Fatigue Crack Propagation in High Strength Aluminum Alloys," Ph.D. thesis, Lehigh University, Bethlehem, Pa., 1965.

[42] A. J. McEvily, Jr., R. C. Boettner, and T. L. Johnston, "On the Formation and Growth of Fatigue Cracks in Polymers," *Fatigue—An Interdisciplinary Approach,* Syracuse University Press, Syracuse, N. Y., 1964.

[43] C. Laird and G. C. Smith, "Crack Propagation in High Stress Fatigue," *Philosophical Magazine,* Vol 7, 1962.

[44] H. W. Liu, "Fatigue Crack Propagation and the Stresses and Strains in the Vicinity of a Crack," *Applied Materials Research,* Vol 3, No. 4, 1964.

[45] G. R. Irwin, "Fracture Mode Transition for a Crack Traversing a Plate," *Transactions,* Am. Soc. Mechanical Engrs., Series D. (*Journal Basic Engineering*), Vol 82, No. 2, 1960.

[46] P. C. Paris, M. P. Gomez, and W. E. Anderson, "A Rational Analytic Theory of Fatigue," *Trend in Engineering,* (University of Washington), Seattle, Washington, Vol 13, No. 1, 1961.

[47] P. C. Paris, "The Fracture Mechanics Approach to Fatigue," *Fatigue—An Interdisciplinary Approach,* Syracuse University Press, Syracuse, N. Y., 1964.

[48] J. Schijve and F. A. Jacobs, "Fatigue Crack Propagation in Unnotched and Notched Aluminum Alloy Specimens," *NLR-TR M.2128,* Amsterdam, 1964.

[49] J. Schijve, A. Nederveen, and F. A. Jacobs, "The Effect of Sheet Width on the Fatigue Crack Propagation in 2024-T3 Alclad Material," *NLR-TR M. 2142,* Amsterdam, 1965.

[50] A. J. McEvily and W. Illg, "The Rate of Fatigue Crack Propagation in Two Aluminum Alloys," *NACA-TN 4394,* 1958.

[51] W. Illg and A. J. McEvily, "The Rate of Fatigue Crack Propagation for Two Aluminum Alloys Under Completely Reversed Loading," *NASA TN-D-52,* 1959.

[52] P. C. Paris, "The Growth of Cracks Due to Variations in Loads," Ph.D. thesis, Lehigh University, Bethlehem, Pa., 1962.

[53] D. Broek and J. Schijve, "The Effect of Sheet Thickness on the Fatigue-Crack Propagation in 2024-T3 Alclad Sheet Materials," *NLR-TR M.2129,* Amsterdam, 1963.

[54] H. F. Hardrath, "Cumulative Damage," *Fatigue—Interdisciplinary Approach,* Syracuse University Press, Syracuse, N. Y., 1964.

[55] J. R. Rice and F. P. Beer, "On the Distribution of Rises and Falls in a Continuous Random Process," *Transactions,* Am. Soc. Mechanical Engrs., Series D (*Journal Basic Engineering*), Vol 87, No. 2, 1965.

[56] J. R. Rice, F. P. Beer, and P. C. Paris, "On the Prediction of Some Random

Loading Characteristics Relevant to Fatigue," *Acoustical Fatigue in Aerospace Structures,* Syracuse University Press, Syracuse, N. Y., 1965.

[57] S. H. Smith, "Fatigue Crack Growth Under Axial Narrow and Broad Band Random Loading," *Acoustical Fatigue in Aerospace Structures,* Syracuse University Press, New York, N. Y., 1965.

[58] H. Hardrath and E. C. Naumann, "Variable Amplitude Fatigue Tests of Aluminum-Alloy Specimens," *Fatigue in Aircraft Structures, ASTM STP 274,* Am. Soc. Testing Mats., 1959.

[59] F. Erdogan and R. Roberts, "A Comparative Study of Crack Propagation in Plates Under Extension and Bending," *Proceedings,* International Conference Fracture, Sendai, Japan, 1965.

[60] A. K. Head, "The Growth of Fatigue Cracks," *Philosophical Magazine,* Vol 44, Series 7, 1953.

[61] A. K. Head, "The Propagation of Fatigue Cracks," *Journal Applied Mechanics,* Vol 23, September, 1956.

[62] F. A. McClintock, "On the Plasticity of the Growth of Fatigue Cracks," *Fracture of Solids,* John Wiley & Sons, Inc., New York, 1963.

[63] J. R. Rice, "Fatigue Crack Growth Model: Some General Comments and Preliminary Study of the Rigid Plastic Strip Model," Lehigh University Institute Research Report, December, 1962.

[64] J. Weertman, "Rate of Growth of Fatigue Cracks as Calculated from the Theory of Infinitesimal Dislocations Distributed on a Plane," *Proceedings,* International Conference Fracture, Sendai, Japan, 1965.

[65] N. E. Frost and D. S. Dugdale, "The Propagation of Fatigue Cracks in Sheet Specimens," *Journal Mechanics Physical Solids,* Vol 6, No. 2, 1958.

[66] H. W. Liu, "Crack Propagation in Thin Metal Sheets Under Repeated Loading," *Transactions,* Am. Society Mechanical Engrs., Series D (*Journal Basic Engineering*), Vol 83, No. 1, 1961.

[67] H. W. Liu, "Fatigue Crack Propagation and Applied Stress Range—An Energy Approach," *Transactions,* Am. Soc. Mechanical Engrs., Series D (*Journal Basic Engineering*), Vol 85, No. 1, 1963.

[68] H. W. Liu, discussion of Ref *47.*

[69] A. R. C. Westwood, "Environment Sensitive Mechanical Behavior—Status and Problems," *Technical Report 65-5,* RIAS (Martin Co.), June, 1965.

[70] N. E. Frost, "The Effect of Environment on the Propagation of Fatigue Cracks in Mild Steel," *Applied Materials Research,* Vol 3, No. 3, 1964.

[71] J. A. Bennett, "Effect of Reactions with the Atmosphere During Fatigue of Metals," *Fatigue—An Interdisciplinary Approach,* Syracuse University Press, Syracuse, N. Y., 1964.

[72] H. C. Rogers, "The Tensile Fracture of Ductile Metals," *Transactions,* Am. Institute Mining, Metallurgical, and Petroleum Engrs., Vol 218, 1960.

[73] F. A. McClintock and F. J. Ryan, "On the Rate of Growth of Fatigue Cracks," *Journal Applied Mechanics,* Vol 76, 1954.

[74] A. A. Wells, "Application of Fracture Mechanics At and Beyond General Yielding," *British Welding Journal,* November, 1963.

[75] L. F. Coffin, Jr., "Low Cycle Fatigue—A Review," *Applied Materials Research,* Vol 1, No. 3, 1962.

DISCUSSION

W. E. Anderson[1] (*written discussion*)—Have you attempted a plasticity solution for the case where the engineering stress-strain curve peaks directly after the elastic portion and decreases continuously to failure?

M. R. Achter[2] (*written discussion*)—Your Class III mode looks as if it might represent high temperature failure. A line scribed on the undeformed specimen surface will be seen, after high temperature deformation, to have an offset at the point where it crosses a grain boundary. From this, it is inferred that adjacent grains suffer shear displacement with respect to each other along the grain boundary plane. Cracks are initiated in these grain boundaries and are propagated inward from the surface. Do you think that you could apply your Class III treatment to the case of intergranular failure at high temperature?

J. C. Grosskreutz[3] (*written discussion*)—Is it possible, at the present stage of elastic-plastic theory, to quantitatively describe the plastic relaxation process observed by Dr. Laird? If so, how would the crack length enter into the crack growth law?

J. R. Rice (*author*)—Upon examining the elastic work hardening plastic anti-plane strain solution for a crack described herein, I find the solution method to fail for the unstable class of stress-strain relations noted by Mr. Anderson. Discrete slip line models appear to be an appropriate model of observed discontinuous yielding when the instability is abrupt as in upper and lower yield point phenomena, but no analysis is available for more gradual relaxations of flow stress with strain. Grain boundary sliding in creep as noted by Dr. Achter could be modelled as a crack with relative motion of surfaces in the two sliding modes, just as such models have been useful in describing the dependence of unconstrained flow and crack nucleation on grain size in the Petch-Stroh analysis of slip line blocking (dislocation pile-up) at a grain boundary.

Dr. Grosskreutz has indicated a very important point in connection with Dr. Laird's observations of striations and their interpretation in terms of a fatigue mechanism. As is clear both from dimensional analysis and the various elastic-plastic models examined herein, a crack growth rate proportional to crack length (more generally, stress intensity factor

[1] Senior supervisor, Fail-Safety-Fracture Mechanics, Commercial Airplane Div., The Boeing Co., Renton, Wash.

[2] Head, High Temperature Alloys Branch, Metallurgy Div., Naval Research Laboratory, Washington, D. C.

[3] Midwest Research Inst., Kansas City, Mo.

squared) will occur if advance is to result purely from a ductile crack opening by sliding off of material at the tip in each load cycle. Further, every striation would then have to be geometrically similar to every other striation (same ratio of spacing to depth). These results are clearly in violation of observations: the general trend of growth rate data is much closer to a proportionality to crack length squared, and Dr. Laird has shown pictures indicating an increasing ratio of striation spacing to depth as crack length or stress level is increased. This raises the question as to whether striations are in themselves indicative of a separation mechanism or are simply observers on the scene. For example, suppose we imagine a ductile material subjected to a cyclic loading while a crack is steadily cut through the material with a razor blade. Striations will result as an inevitable consequence of the cyclic loading combined with a material capability for permanent deformations, but they then have nothing to do with the separation mechanism. This is precisely the problem with Dr. Laird's suggestion that striation markings necessarily indicate a mechanism of separation in fatigue—other interpretations are possible. In particular one interpretation is that the observation of striations simply means that crack opening displacements (approximately equal to striation depth) are comparable in size to the growth increment per cycle (striation spacing). Indeed, application of Eqs 43*b*, 44, and 45 for crack opening displacements to the data for the two aluminum alloys of Figs. 24 and 25 gives a prediction of opening displacements comparable in size to the measured growth per cycle over the middle range of the data in both cases. From the plane strain slip line field for a sharp crack in Fig. 21, it would appear that large strains can occur directly in front of the crack only if the tip is rounded. Thus crack opening displacements are indicative of the size of the highly strained region in front of the crack, so that a growth rate per cycle roughly comparable in size to opening displacement is not unexpected. Still, the general trend of growth rate data shows clearly that the growth per cycle is not directly proportional to crack opening displacement, as required in Dr. Laird's interpretation. A length parameter characterizing the material must enter as discussed in the last section of the paper.